



TECHNISCHE
UNIVERSITÄT
WIEN

DIPLOMARBEIT

Development of a Human *in vitro* Cystic Fibrosis Model for Personalized Medicine

Thema

Ausgeführt am Institut für

E163 Institut für Angewandte Synthesechemie
E164 Institut für Chemische Technologien und Analytik

der Technischen Universität Wien

unter der Anleitung von Univ. Prof. Dipl.-Ing. Dr. Peter Ertl und Dr. Janna Nawroth

B.Sc. Doris Roth

Name

Datum

Unterschrift (Studentin)



Die approbierte gedruckte Originalversion dieser Diplomarbeit ist an der TU Wien Bibliothek verfügbar
The approved original version of this thesis is available in print at TU Wien Bibliothek.



TECHNISCHE
UNIVERSITÄT
WIEN



CELLCHIP
GROUP

Development of a Human *in vitro* Cystic Fibrosis Model for Personalized Medicine

Master Thesis

Author: Doris Roth

First Supervisor: Prof. Dr. Peter Ertl

Second Supervisor: Dr. Janna Nawroth

August 2021

Vienna University of Technology

Faculty of Technical Chemistry

Institute for Applied Synthetic Chemistry & Institute for Chemical Technologies and Analytics

Cell Chip Group

Conducted at Emulate Inc. Boston, MA, USA

Abstract (English)

Engineered human microtissues provide an unparalleled window into structure-function relationships that underlie organ function, drug responses, and pathologies. The aim is to recapitulate both native tissue architecture and the organotypic mechano-chemical microenvironment to enable the study of dynamic interactions, emergent functions and disease states, such as in Cystic Fibrosis (CF). Specifically, engineered CF lung microtissues can help identify disease mechanisms and develop diagnostics for symptomatic and etiological treatment and the treatment of the onset and progression of the most common lethal infection with *Pseudomonas aeruginosa* in CF disease. Here, I discuss the development of a patient cell-based *in vitro* model of CF airway inflammation, the Cystic Fibrosis-Airway-Chip, that emulates and enables the patient-specific, real-time study of the interactions between mucociliary function, immune cell responses and bacterial infection onset and progression. This work led to a reproducible healthy and CF patient-derived epithelial tissue culture on a microfluidic chip, showing basal cells, mucus secreting goblet and club cells, as well as ciliated cells. Video microscopy revealed ciliary beat and mucociliary transport of fluorescent beads that was locally distorted in CF donors, in line with impeded mucociliary clearance observed in the CF lung. In the future, such a model can help understanding the role of patient-specific inflammatory responses and immune cell recruitment in shaping cystic fibrosis disease states.

Abstract (Deutsch)

Gezüchtete humane Mikrogewebe ermöglichen einen beispiellosen Einblick in die Struktur-Funktions-Beziehungen von Organen, die Arzneimittelreaktionen und Pathologien zugrunde liegen. Ziel ist es, sowohl die native Gewebearchitektur als auch die organotypische mechanochemische Mikroumgebung, wie Konzentrationsgradienten und Scherkräfte, nachzuahmen, um die Erforschung dynamischer Wechselwirkungen und folglich Funktionen sowie Pathologien, möglichst nah an der menschlichen Biologie zu ermöglichen.

Speziell kultivierte humane Lungenmikrogewebe tragen dazu bei, Krankheitsmechanismen zu identifizieren und Strategien für die symptomatische und ätiologische Behandlung, sowie die Behandlung des Beginns und des Fortschreitens tödlicher Infektionen, zu entwickeln. Diese Arbeit zeigt die Entwicklung eines patientenzellbasierten *in-vitro*-Modells der Atemwegserkrankung Mukoviszidose (Zystische Fibrose; Cystic Fibrosis - CF), des Cystic Fibrosis-Airway-Chips. Dieser Chip ermöglicht die patientenspezifische Echtzeit-Untersuchung der Wechselwirkungen zwischen Schleimhautfunktion, Immunzellreaktionen und bakteriellem Befall sowie Infektionsbeginn und -verlauf. Hierzu wurde eine reproduzierbare gesunde und von CF-Patienten stammende pulmonale Epithelgewebekultur auf einem mikrofluidischen Chip entwickelt. Mittels Immunfluoreszenzfärbung konnten Basalzellen, Schleim produzierende Becher- und Keulenzellen, sowie Kinozilien-tragende Zellen nachgewiesen werden. Die Verwendung von Videomikroskopie zeigte das Schlagen dieser Kinozilien und den mukoziliären Transport von fluoreszierenden Partikeln, der im Vergleich zum gesunden Epithel, lokale Störungen in CF Kulturen, im Einklang mit der beobachteten Beeinträchtigung der mukoziliären Clearance in Mukoviszidose PatientInnen, aufwies. Dieses Modell liefert einen wichtigen Beitrag zum Verständnis der Rolle von patientenspezifischen Entzündungsreaktionen und Immunzellrekrutierung, sowie der tödlichen Infektion mit *Pseudomonas aeruginosa* im Krankheitsverlauf von Mukoviszidose.

Acknowledgments

I want to thank my supportive thesis supervisor, Prof. Peter Ertl, for his guidance since the day that I walked into his office and told him about my plans to conduct my thesis abroad. Thank you for introducing me to the scientific world and community. I also want to give my sincerest gratitude to Professor Laurence G. Rahme at Massachusetts General Hospital and Harvard Medical School for all of her effort so that I could conduct this work. Thank you to Dr. Geraldine Hamilton, Dr. Katia Karalis, and Emulate Inc. for granting me the opportunity to travel to Boston and work at this company. Thank you for all the resources I was so generously offered.

Dr. Janna Nawroth, you didn't know me at all, but you trusted me and agreed to be my supervisor at Emulate Inc. – a risky move, but we nailed it. Thank you so much for all your support, guidance, and help. Thank you for all the interesting and funny conversations and moments. You know how to spark joy and curiosity in others – this is so special! Dr. Anne van der Does, without you, I would have been lost. Thank you for basically everything. You two are inspiring and brilliant female scientists whom I am so proud to work with and look up to. I want to thank you from the bottom of my heart.

Coco and Alex, you made this possible, you were there. I am full of gratitude, and my heart is filled with love for you. Andi, thank you for - running - the final miles with me. You taught me so much in such a short time, academically but most important personally. You make my heart smile.

Coco, Alex and my partner Andi – people to whom I want to apologize in advance for my decision to write a doctoral thesis in a few years.

Content

0	List of Abbreviations.....	9
1	Introduction	11
1.1	The Immune System, <i>Pseudomonas aeruginosa</i> , and the Cystic Fibrosis Airway.....	12
1.2	Current Airway models.....	13
1.3	Organs-on-a-Chip	15
1.4	Lung-on-a-chip.....	16
1.5	Approach	19
2	Materials and Methods.....	20
2.1	Organ Chips.....	20
2.2	Instrumental Setup.....	22
2.3	Chip Fabrication.....	24
2.4	Healthy primary airway epithelial cell culture.....	25
2.4.1	Cell Expansion.....	25
2.4.2	Transwell Controls	27
2.4.3	S-1™ Chip cultures.....	27
2.5	Cystic Fibrosis airway epithelial cell culture	31
2.5.1	Cell Expansion.....	31
2.5.2	ECM coating	33
2.5.3	Transwell culture.....	33
2.5.4	Chip cultures.....	34
2.5.5	Open Top Chip Culture	34
2.5.6	S1-Chip culture	35
2.6	Immunofluorescence Staining	35
2.7	Lactate Dehydrogenase Cytotoxicity Assay	36
2.8	High-Speed Video Microscopy	36

2.9	Cilia Imaging.....	36
2.10	Bead Transport.....	37
2.11	Image Analysis	37
3	Results.....	38
3.1	Emulating the Healthy Human Airway	38
3.2	Emulating the Cystic Fibrosis Airway	45
4	Discussion	53
5	Conclusion	55
6	References	57
7	Table of figures	62
8	Attachments.....	66

0 List of Abbreviations

ALI	air liquid interface
ASL	airway surface liquid
BEBM	bronchial epithelial cell growth basal medium
BSA	bovine serum albumin
BTEC	bronchial tracheal airway epithelial cell
CAD	computer-aided design
CC16	club cell secretory protein
CF	Cystic Fibrosis
CFTR	cystic fibrosis transmembrane conductance regulator
col I, IV	type I, IV collagen
COPD	chronic obstructive pulmonary disease
CRISPR-Cas9	clustered regularly interspaced short palindromic repeats - CRISPR associated protein 9
DAPI	4',6-diamidino-2-phenylindole
DMEM	Dulbecco's Modified Eagle Medium
DNA	desoxyribonucleic acid
EC-23	4-[2-(5,6,7,8-Tetrahydro-5,5,8,8-tetramethyl-2-naphthalenyl)ethynyl)- benzoic acid
ECM	extracellular matrix
EDC	1-Ethyl-3-(3-dimethylaminopropyl)carbodiimide
ELISA	enzyme-linked immunosorbent assay
EMT	epithelial-mesenchymal transition
ENaC	epithelial sodium channel
hEGF	human epithelial growth factor
IgG	immunoglobulin G

IL- β , IL-8, IL-13	interleukin β , 8, 13
iPSC	induced pluripotent stem cell
LDH	lactate dehydrogenase
Muc5AC	mucin 5AC
NET	neutrophil extracellular trap
NHS	N-Hydroxysuccinimid
OOC	Organ-on-a-chip
OT chips	Open Top chip
<i>P. aeruginosa</i>	<i>Pseudomonas aeruginosa</i>
p63	tumor protein 63
PBEC	primary normal human bronchial airway epithelial cell
PBS	phosphate buffered saline
PCL	periciliary liquid
PDMS	polydimethylsiloxane
PET	polyethylene terephthalate
PWM	pulse width modulation
qPCR	real-time quantitative polymerase chain reaction
SAEC	primary normal human small airway epithelial cell
SAGM	small airway epithelial cell growth medium
TNF- α	tumor necrosis factor α
VEGF	vascular endothelial growth factor
ZO-1	zonula occludens 1

1 Introduction

In cystic fibrosis (CF) patients, genetic mutations in the cystic fibrosis transmembrane conductance regulator (CFTR) gene (Cytogenetic Location: 7q31.2) cause multiple organ manifestations such as pancreatic insufficiency, diabetes, and obstructive lung disease from infancy with chronic bacterial infections, with lung disease representing the leading cause of morbidity and mortality[1]. The critical disease manifestations in the human lung are delayed mucociliary clearance through airway surface liquid depletion, abnormalities of the physical properties and adhesion of mucus, predisposition to chronic microbial infection due to abnormal mucosal defenses, and dysregulated inflammation that almost always leads to irreversible lung injury[1]. While it is well-known that a combination of these factors underlies the initiation and perpetuation of chronic infection and inflammation, the precise role and timing of individual factors remain unclear. In particular, due to the lack of suitable animal and *in vitro* models of CF airways, we do not fully understand whether destructive airway inflammation is a consequence or can also be the cause of increased susceptibility to chronic infection[1]. A recent study suggests that early CF lung disease is characterized by an increased mucus burden and inflammatory markers without infection or structural lung disease[2].

In the human bronchial and small airway epithelium, ciliated cells are highly polarized and beat their cilia in a coordinated fashion through a lubricating substance, the periciliary liquid (PCL). This PCL-lubricated ciliary beat enables the unidirectional and efficient transport of the overlying mucus secreted by interspersed goblet cells. The so-called mucociliary escalator traps and clears pathogens and toxins out of the lungs and is essential for physiological lung function. The perturbation of CFTR-mediated fluid secretion and ion gating alters the salt composition of the mucus and, in consequence, increases mucus viscosity[3], [4]. Due to the increased "stickiness" of the mucus, mucociliary transport is significantly impaired, which is hypothesized to generate mucus buildup that not only impedes breathing but also renders the patient susceptible to chronic lung infection with pathogens, particularly the bacterium *Pseudomonas aeruginosa*[5]–[7].

Furthermore, CFTR defects are known to increase fluid and sodium absorption via the epithelial sodium channel (ENaC), which is thought to exacerbate the depletion of the lubricating periciliary layer and further impair mucociliary transport[8]. According to one hypothesis, the great sensitivity of the periciliary layer to the altered osmolar forces of the overlying mucus eventually causes the periciliary layer to collapse, ensuing in failure of mucociliary transport[9]. The stagnant mucus environment could thus enable pathogens, such as *P. aeruginosa*, to take hold and form

permanent biofilms[7], [10]. In addition, decreased bicarbonate transport through CFTR is thought to condense the mucus and lower the pH in the human airway, which may affect host immune cell activities and contribute to deficiencies in pathogen defense[11]–[13]. CF epithelium may elicit resident immune cell activation even without the presence of infections, causing harmful immune responses[1], [2], [14], [15]. Conversely, the presence of bacterial biofilms, in turn, could elicit harmful immune responses and cause tissue remodeling that further impairs mucociliary transport[16].

In sum, mucociliary transport, *P. aeruginosa*, and host immune cells engage in very complex interactions in CF airways, and their sequence and causalities remain unclear. Further, while Cystic Fibrosis is caused by the defect of a single gene, according to the CFTR2 database (<https://cftr2.org/>), 346 different CF-causing mutations have been identified, each of which might change the relative role of the factors involved in lung pathogenesis. Since the discovery of the gene defect in 1989, published in a series of three publications[17]–[19], more than 2000 genetic variants of CFTR have been discovered. Different mutations and combinations of mutations cause different disease phenotypes in an autosomal recessive monogenetic fashion, with the F508del variant being the most common mutation causing Cystic Fibrosis[20]. High variability in phenotype and a broad range of disease severity is observed even in patients carrying the same genotype[21].

This master thesis aims to address these challenges by developing a patient-cell-based dynamic 3D *in vitro* model of the CF airway, the CF Airway Chip, that recapitulates and enables the patient-specific, real-time study of the interactions between mucociliary function, immune cell responses, and bacterial infection onset and progression. Furthermore, biomechanical readout methods have been developed to describe the CF mucociliary escalator.

1.1 The Immune System, *Pseudomonas aeruginosa*, and the Cystic Fibrosis Airway

The airway epithelium, the immune system, and the pathogen *Pseudomonas aeruginosa* engage in complex interactions leading to disease exacerbations and mortality in patients with Cystic Fibrosis. The respiratory tract is home to many resident and circulating immune cells, including natural killer cells, macrophages, mast cells, dendritic cells, neutrophils, and lymphocytes that continuously protect the lung tissue from pathogens and foreign particles entering the lung[22]. In CF patients, unresolved neutrophilic inflammation and recurrent pulmonary infections lead to lung disease, disease exacerbations, and structural lung damage.

Studies show that even in the absence of infection with pathogens, abnormalities of the CF airway mucus, such as increased viscosity, can already lead to a proinflammatory environment, hypoxia, and oxidative stress[2]. Excessive neutrophil-dominated inflammation is observed[1], and neutrophil elastase activity was associated with early bronchiectasis in children[23]. Findings of elevated neutrophil elastase levels and other inflammatory markers such as IL- β , IL-8, and TNF- α in the airway and studies on CF fetuses suggest that inflammation precedes infection. In contrast, other studies argue that inflammation is secondary to infection[24].

Chronic neutrophilic-mediated inflammation following infection can markedly reduce airway surface liquid (ASL) height[1], [25], affecting the mucociliary escalator. Further, the accumulation of large amounts of DNA derived from neutrophils and actin increases mucus viscosity and negatively impacts mucociliary clearance[24]. A vital component of this dysregulation is NETosis, a particular form of cell death that leads to the release of neutrophil extracellular traps (NETs). NETs are networks of primarily DNA and actin associated with granules, such as the protease neutrophil elastase, that trap pathogens[26]. In CF, neutrophils and *P. aeruginosa* induced NETs are incapable of clearing the infection and, in fact, even favor bacterial colonization and the formation of biofilms, leading to an environment where clinical strains can acquire resistance to NET-mediated killing[24]. *P. aeruginosa* can undergo microevolution and adapt to develop multi-drug resistance, as shown in the analysis of isolated strains from a CF patient throughout eight years[27]. The microaerophilic environment of the CF lung presents a hostile environment to *P. aeruginosa*, resulting in the formation of low oxygen tension biofilms[28], [29]. *P. aeruginosa* biofilms are associated with excessive inflammation, recurrent exacerbations, accelerated lung function decline and ultimately increasing mortality. To date, no effective treatment options for recurrent *P. aeruginosa* infection in CF exist. And hence, platforms that enable the study of host-pathogen interaction upon infection of the CF airway, biofilm formation, dysregulated immune reaction, elevated neutrophil infiltration, and NETosis in the human body are desperately needed.

1.2 Current Airway models

Cystic Fibrosis research is performed in various animal and *in vitro* models essential for drug discovery, drug testing, and foundational research. Each model has specific advantages and challenges when mimicking the human physiology of the CF lung (fig 1). Soon after the discovery of CFTR, CF mouse models were developed, and mice are now widely used model organisms for CF research, especially for the intestine. However, mice models homozygous for the most common F508del mutation were thought to not show any abnormalities in lung function[30].

Recent studies suggest that CF mouse models do show particular abnormalities in lung function but fail to mimic the severity and scope of the human disease condition[31].

Furthermore, the tissue composition and function differ vastly between mice and humans, including differences in epithelial cell composition, cartilage architecture, smooth muscle biology and altered electrophysiology[31]. For example, the proportions of mucus-producing goblet cells, secretory club cells, and ciliated cells differ between mice and humans[31]. Lastly, mouse models infected with human pathogens do not recapitulate a CF patient's disease states and infection response, hence insufficiently representing the complex nature of host-pathogen interactions in humans[31].

Other animal models such as the CF pig and CF ferret recapitulate the full spectrum of CF phenotype in human patients and closely resemble human lung cell biology[32]. The CF ferret covers a wide range of abnormal airway functions for the study of CF but does not exhibit ENaC dysregulation, and disease severity is significantly increased compared to humans. Both the CF ferret and the CF pig require high maintenance and intensive medical treatment to improve their lifespan[31]. CF rats are promising model organisms but need further characterization.

Human *in vitro* airway cell models are increasingly being used in CF research with human cells cultured at air liquid interface on transwell™ supports to resemble human biology more closely. This technique emerged as the gold standard for airway *in vitro* models and replaced undifferentiated submerged 2D cultures. Immortalized cell lines like Calu-3 from adenocarcinomas or CRISPR-Cas9 gene-edited cell lines are used to study the role of CFTR[32]. The more preferred and used *in vitro* model for CF research are primary cells, progenitor cells obtained from human tissue and differentiated into pseudostratified airway epithelium[33]. Although challenging, there are promising approaches for using differentiated induced pluripotent stem cells (iPSCs) for airway *in vitro* models[32], [34].

Among those exceptional advances in stem cell research are organoids. Lung organoids are derived from progenitor cells that self-assemble to form differentiated tissue spheroids with an internal lumen[35]. The organoid technology enables the easy testing of the efficacy of CFTR modulator and corrector drugs using a swelling assay, where the recovery of CFTR function is indicated by an increase of the luminal diameter in intestinal organoids[36], [37]. These new approaches in 3D cell culture models are accompanied in their novelty by the organ-on-a-chip technology and, more specifically, in the context of the healthy airway, the small airway-on-a-chip[38], [39]. Organ chips are 3D *in vitro* microfluidic cell culture platforms that emulate the

mechanochemical microenvironment and the 3D architecture of human tissue. Dynamic chip cultures resemble *in vivo* human physiology more closely compared to static 3D transwell cultures. A more detailed description of the Airway-Chip can be found in section 2.1.

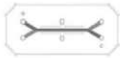
					
	Animal	Lung-on-Chip	Organoid	Air Exposed Primary Cells	2D Cell Line
3D tissue architecture	●●●	●●○	●●○	●○○	○○○
Full cell differentiation	●●●	●●○	●●○	●●○	●○○
Hemodynamic environment	●●●	●●●	○○○	○○○	○○○
Circulating immune cells	●●●	●●○	○○○	●○○	○○○
Physiological biomechanics	●●●	●●○	●○○	●○○	○○○
Long-term viability	●●●	●○○	●●○	●●○	●●●
Familiarity	●●●	●○○	●●○	●●●	●●●
Access to luminal space	●●○	●●●	●○○	●●●	○○○
Patient-specific cells	●○○	●●●	●●●	●●●	●●●
Conserved disease phenotype	○○○	●●○	●●○	●○○	●○○
Throughput	○○○	●○○	●●○	●●○	●●●

Figure 1: Comparison of experimental strategies for lung modeling taken from Nawroth et al. 2018 [40]. Whereas animal models enable *in vivo* studies, they do not resemble human physiology and, in particular, diseased phenotypes. High maintenance efforts and the ethical need to minimize the use of animals lower the throughput of studies. The Lung-on-Chip uses human cells that can be patient-specific and incorporates differentiated epithelium and endothelium as well as circulating immune cells. The microfluidic channels in the chip create tissue-tissue interfaces and mimic the *in vivo* hemodynamic environment. The complexity and novelty of the chip reduce the throughput and familiarity. Organoid cultures self-assemble and allow the study of patient-derived airway epithelium. The spheroid shape with an internal lumen excludes infection modeling and the study of mucociliary clearance. Air exposed primary cells in transwell cultures have standardized culture protocols and are easy to use. Transwell cultures are highly characterized and allow the use of patient-specific cells. The static culture model does not mimic the mechanical microenvironment crucial for complete differentiation, especially for endothelial cells. 2D submerged cell lines are of great use for CFTR-related research but highly limited for translational research.

1.3 Organs-on-a-Chip

Organs-on-a-chips (OOCs) are engineered microtissues coupled with microfluidic devices emulating native tissue architecture and the mechanochemical environment of an organ. OOCs emerged from parallel advances in microfabrication in the semiconductor industry, stem cell technology, and human tissue engineering. The microenvironment includes multiple cell types enabling tissue-tissue interfaces and controlled involvement of mechanical forces such as stretch and shear, fluid flow, biochemical cues, and electrical or optical signals [40]–[43]. The design of OOCs is guided by the applications that the organ model should host, such as crucial physiological functions and readouts with spatio-temporal resolution. Hence, they do not attempt

to mimic an entire organ. The goal is to provide a complex physiological model, yet one simple enough to facilitate reproducibility, manipulation and control.

When mimicking physiological barriers, cells are growing on porous membranes inside the chip within interfacing microfluidic channels. This enables cell-cell and tissue-tissue interactions that exceeds conventional 2D culture models by far. This is crucial in the context of complex disease models and it has been shown that endothelial and mesenchymal cells modulate the differentiation of epithelial cells towards the development of adult airway epithelium [40], tissue growth, and cell activation during inflammation.

The ability to perfuse OOCs enables the incorporation of circulating immune cells that can migrate to the epithelium upon the activation of the underlying endothelium[42], and the dynamic flow of nutrient-containing liquids and gases exerts shear stresses as those experienced within small vessels[44] adding further to their physiological relevance. Endothelial cells are constantly exposed to forces, such as gravitational forces, mechanical stretches, stress, and shear stress. Physiological shear stress experienced through blood flow and the flow pattern has been shown to modify morphology, gene expression, and metabolism of endothelial cells[45]–[47]. In addition, the lung epithelium is subject to dynamic stresses, stretches, and pressure changes during breathing. It has been shown that low levels of shear stresses enhance epithelial barrier function[48], and mechanical forces experienced by the epithelium are critical regulators during lung development[49]–[51].

The small-airway-on-a-chip described by Benam et al.[52] consists of differentiated mucociliary airway epithelium and a microvascular endothelium in a manipulatable mechanical environment with nutrient flow through the endothelial channel. This model is the base for the development of the Cystic Fibrosis chip.

1.4 Lung-on-a-chip

The primary function of the human lung is gas exchange. The aspirated air flows through the conducting airways, where it gets humidified and warmed. The air then reaches the alveoli, the gas exchanging regions of the lung. The lung is highly branched, and the epithelium is characterized by a continuous transition in cell type composition. First, air is conducted through the trachea into the two main bronchi, lined by tall columnar epithelium and transitioning into pseudostratified epithelium, containing seromucous glands. Next, the conducting airways branch into the bronchioles and finally terminal bronchioles. The first generations of the bronchioles show a high proportion of mucus-secreting goblet cells, ciliated cells, and non-ciliated basal cells.

Ciliated cuboidal epithelium is observed in the terminal bronchioles, and mucus-secreting club cells appear and increase in number while goblet cells are not present anymore. Ultimately, the terminal bronchioles branch to form the respiratory portion of the lung, namely the respiratory bronchioles, the alveolar ducts, the alveolar sacs, and finally, the alveoli. The two main cell types present in the alveolus are type I pneumocytes, large flat cells at times only a few nanometers thick for gas exchange, and type II pneumocytes, that secrete surfactant to reduce surface tension of the alveoli and prevent them from collapsing[53]. The lung is heavily vascularized in order to facilitate efficient gas exchange. Cartilage is only present in the trachea and bronchi, while smooth musculature can be found until the alveolar duct, regulating the luminal diameter.

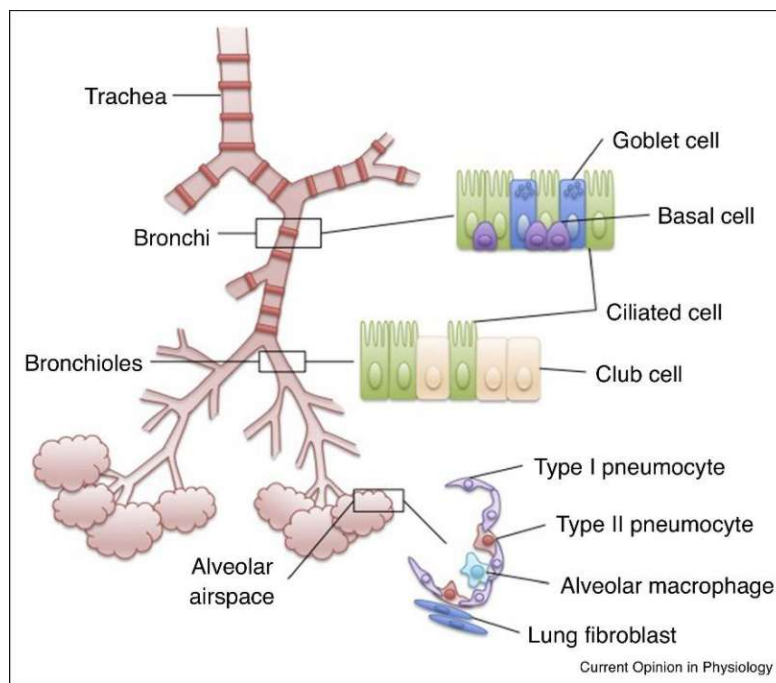


Figure 2 Branching and epithelial composition of the human lung [53]

Regarding this highly hierarchical and complex organ, it is easy to comprehend that different lung diseases have different starting points and pathogenesis due to tissular and epithelial composition. As a prominent current and urgent example, the coronavirus disease 2019 pandemic poses a huge and pressing challenge for the research community and chip models of the different regions of the lung, as the disease states are thought to correlate with the site of the infected epithelium[54], [55], can have a massive impact on the understanding of the disease mechanisms and ultimately on the treatment of patients. Cystic Fibrosis, is characterized by epithelial surface liquid depletion and hence viscous mucus impeding the mucociliary clearance, rendering the patients susceptible to otherwise nonlethal pathogens[1]. In order to face these challenges,

different models of the human airways representing different epithelial cell type compositions together with healthy and altered mechanochemical environments are needed.

Several research groups developed lung-on-a-chip models and used healthy cultures as a base for disease modeling. A milestone was set by paper by Benam et al. in 2016[52] when they described the development of an IL-13 induced chronic inflammation model of the small airway, namely the small-air-way-on-a-chip, that aims to mimic asthma and chronic obstructive pulmonary disease (COPD) and which showed similar inflammatory responses as *in vivo*, such as goblet cell hyperplasia and elevated inflammatory markers. In this barrier chip, two PDMS channels are separated by a PET membrane, and pseudostratified small airway epithelium is cultured on air on the membrane. Microvascular endothelium is constantly perfused on the other side of the membrane. Thus, they were able to build a more robust model as compared to previous ones[56]. This paper was based on one of the first organs-on-a-chip papers mimicking the alveolar-endothelial barrier published in Science by Huh et al. from 2010[42], where additionally to the two culture chambers, lateral vacuum chambers were introduced to actuate the membrane and mimic physiological stretch experienced by the tissue. Nesmith et al. developed a human airway musculature on a chip to mimic allergic asthmatic bronchoconstriction and dilation[57]. The musculature was cultured on thin films that deflected upon muscle contraction. IL-13 induced inflammation resulted in hypercontractility, and muscarinic antagonist and a β -agonist, which are used clinically to relax constricted airways, lead to muscle release. A study from 2017 by Hassel et al.[58] reports a non-small-cell lung cancer chip model using a barrier chip setup. They showed that cyclic breathing motion reduced tumor growth significantly, thereby indicating a direct relation between tumor dormancy and impeded lung mechanics. Nevertheless, the role of physical forces and tissue properties in lung biology are yet not well understood. While mechanical stresses are thought to stimulate lung growth[59] and regeneration after injury[60], the same forces can cause long-lasting damage in the context of mechanical ventilation[61]. In a recent study by Nawroth et al. from 202, mimicking breathing on a barrier chip containing a flexible 7 μm pore PDMS membrane by using cyclic strain at physiological levels and directed airflow, increased club cell number, possibly skewing the human primary bronchial airway culture towards a small airway phenotype. Further breathing-associated mechanical stimulation led to reduced IL-8 secretion and downregulated gene expression of matrix metalloproteinase 9, fibronectin, and other extracellular matrix (ECM) factors[62].

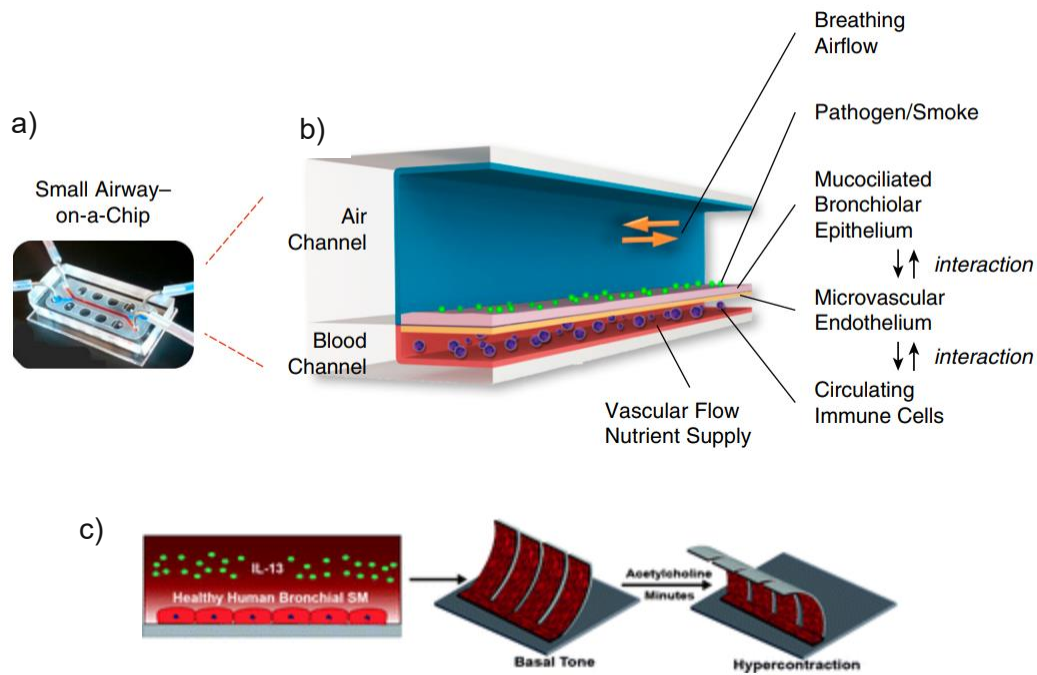


Figure 3 a); b) barrier chip by Benam et al. [63] c) thin film airway musculature by Nesmith et al.[57]

A barrier chip, where two channels are separated by a porous membrane with vacuum channels along both channel sides to mimic breathing strain, is predominantly used in disease modeling [64] mainly because lung diseases often affect not only the epithelium but also the endothelium, e.g., thrombosis[65] and edema[66], and further because it allows for immune cell recruitment[55]. The complexity and variety of conditions, as well as the strong influences of mechanical forces on pulmonary biology highlighted in these works, demonstrate the necessity of further development of airway chips. Chips mimicking the larger airways, such as a trachea-on-a-chip or bronchus-on-a-chip, and chips emulating the small airways as well as the respiratory portion have a strong potential in shaping our future understanding of pathophysiology and, in consequence, treatment options.

1.5 Approach

In order to develop a Cystic Fibrosis on-chip model, the first step is to establish a healthy control chip culture to create a reference. While the healthy airway culture on a chip provided by Emulate Inc. (S-1 chip) undergoes optimization, the obtained knowledge of the healthy model is used to develop the diseased model (fig 2). This thesis focuses on establishing methods to differentiate healthy and patient-derived Cystic Fibrosis primary airway epithelial cells on the S-1 chip, so as

to break down complexity and narrow down the multitude of parameters that goes along with organ modelling. Parameters that are assessed are extracellular matrix composition for cell attachment to the chip membrane, hydrogel-based barriers, cell culture medium and supplements, flow conditions and in the case of the disease model membrane material, as membrane stiffness is linked to cell viability and differentiation.

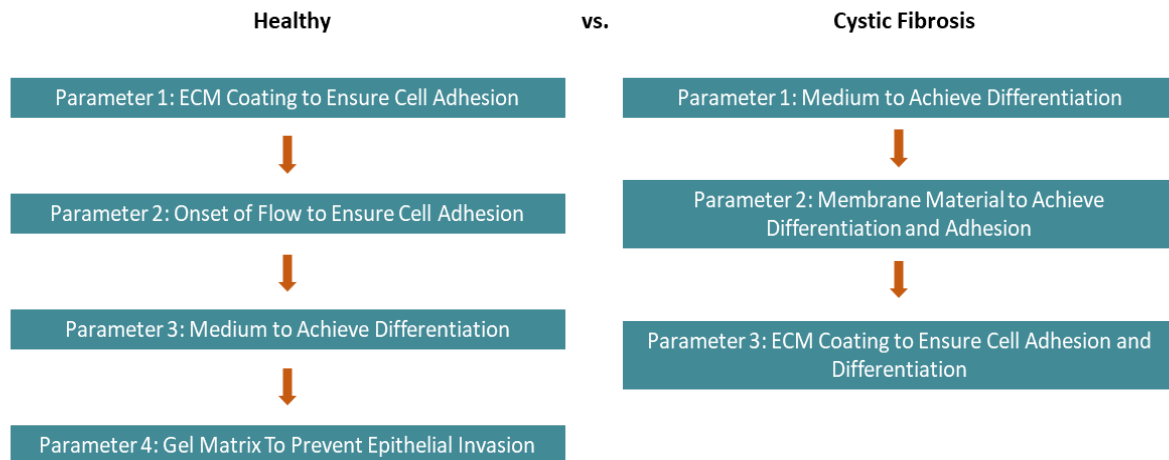


Figure 4: Steps in model development

2 Materials and Methods

2.1 Organ Chips

Four different *in vitro* cell culture platforms were used to differentiate airway epithelial cells (fig 3). Transwell plates (Corning, USA) were used as static controls where a transwell insert with a permeable 0.4 μm pore polyester membrane is hanging into a well. The resulting two compartments can be accessed independently and allow for submerged culture conditions and air liquid interface that is needed to differentiate airway cells. Emulate Inc. provided organ chips. The stretchable Organ-Chip S-1TM consists of a top channel and a bottom channel separated by a porous membrane, and dynamic laminar flow conditions can be set independently for both channels. Two different types of membranes were used. The standard S-1 design carries a 7 μm pore polydimethylsiloxane (PDMS) membrane, and the alternative design[52] uses a polyethylene terephthalate (PET) with pores exhibiting an average diameter of 3 μm . The PET membrane is stiffer than the PDMS membrane, but due to its fabrication leading to random distribution of the pores and occasionally merging pores, the pore size can vary from 3 μm to up to 10 μm . The

pores in the PDMS membrane are hexagonally packed and distributed evenly. Another benefit of the PDMS membrane is its optical clarity which is limited in PET and can hinder optical readouts. The Open Top Chip[67] has a spiral microfluidic bottom channel and a top channel leading through a hard-plastic gasket that connects to an open chamber. The open chamber can easily be accessed by removing the gasket and it sits on top of a spiral bottom channel. The two channels are divided by a 7 μm pore PDMS membrane.

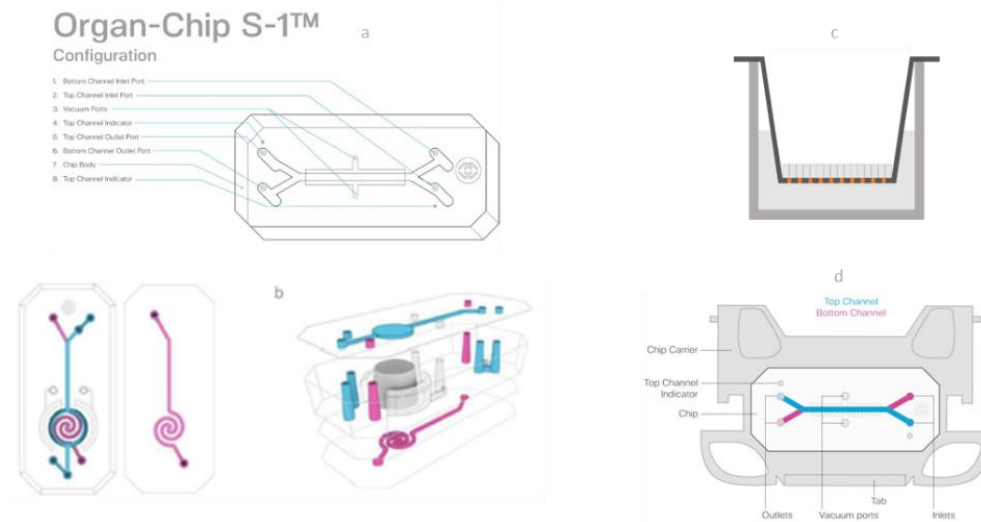


Figure 5: Cell Culture Platforms a) S1-Chip Design with PET or PDMS membrane b) Open Top Chip Design with PDMS membrane c) transwell with PET membrane d) S1-Chip in chip carrier

Table 1: Dimensions of the S1-Chip

Top Channel	
Width x height dimensions	1000 μm x 1000 μm
Area	28.0 mm^2
Volume	28.041 μL
Imaging distance from bottom of chip to top of membrane	850 μm
Bottom Channel	
Width x height dimensions	1000 μm x 200 μm
Area	24.5 mm^2
Volume	5.6 μL
Membrane	
Pore diameter	7.0 μm
Pore spacing	40 μm (hexagonally packed)
Thickness	50 μm
Co-Culture Region	
Area	17.1 mm^2

The base model of the airway chip (fig 4) consists of a mucociliary airway epithelium in the top channel, or chamber for Open Top-Chip, and a microvascular endothelium in the bottom channel. The top channel is submerged or kept at air under static conditions for differentiation, and the bottom channel is constantly perfused with fresh medium mimicking human vessels.

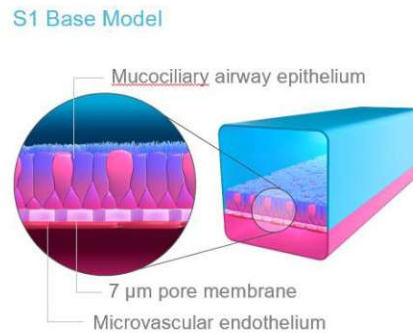


Figure 6: Emulate S1-Chip with Airway Culture: The top channel and bottom channel are separated by a 7 µm pore PDMS membrane. The top channel houses the mucociliary airway epithelium and microvascular endothelium is seeded to the bottom channel. Both channels can be perfused with different fluids/air and at different flowrates.

2.2 Instrumental Setup

The Human Emulation System of Emulate Inc. was used to perform the on-chip experiments. The components of the Human Emulation System consist of a Pod™ that houses the organ-chip, the Zoë-CM1™ module that provides pressure-driven laminar flow as well as stretch, and the Orb-HM1™ that delivers a mix of 5% CO₂ with air, vacuum, and power (fig 5). The Pod's top and bottom channel reservoirs hold up to 4 ml of medium that reaches the chip through an embedded microfluidic resistor. The Pod is equipped with a window above the chip that allows for imaging. Apart from its function as a media reservoir, it also serves as the interface between chip and Zoë. Zoë holds up to 12 chips, provides independent laminar medium flow for top and bottom channels, and supplies vacuum for a mechanical stretch at tunable frequencies and amplitudes. Zoë also features a prime cycle that primes the microfluidic channels of the Pod and creates liquid droplets on the ports for chip connection. The "regulate cycle" applies pressure to chips and Pods to eliminate any air bubbles in the system that could interfere with medium flow. The mix of 5% CO₂ and air for medium flow as well as vacuum (-70kPa) for stretch is provided through the Orb that forms a hub for up to four Zoës.

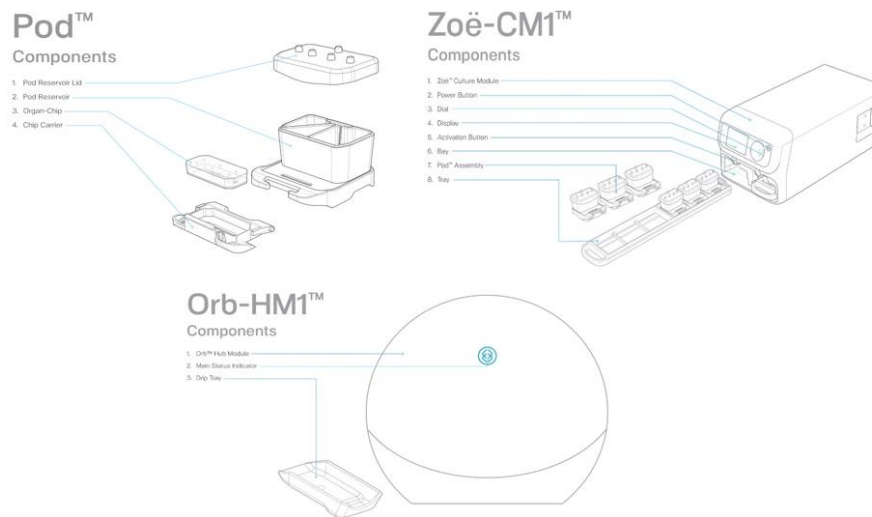


Figure 7 The Human Emulation System Components Pod, Zoë and Orb

The flow rates can be set for both channels individually (fig 6). The Airway chip flow rates are set to 30 μL per hour for both channels during the submerged phase and 0 μL per hour on the top channel and 30 μL per hour on the bottom channel from the introduction of air liquid interface onwards. The low flow rate of 30 μl per hour is achieved by using pulse width modulation (PWM), where 2.2 kPa or 0 kPa are applied to the Pods at a period of 10 seconds resulting in an average flow rate of 30 μl per hour. The peak pressure has a duty cycle of 17.4%. The applied pressure drops significantly due to the long microfluidic resistor (60 cm) before entering the chip where it is close to zero. No pressure is applied to the outlet reservoirs during regular flow. The resistance is given as PodID (PodID = 54) and equals $\frac{1}{R}$ when used in Ohm's law to calculate flow rates (Q).

$$Q = \frac{\Delta P}{R} \leftrightarrow Q = \Delta P \cdot PodID$$

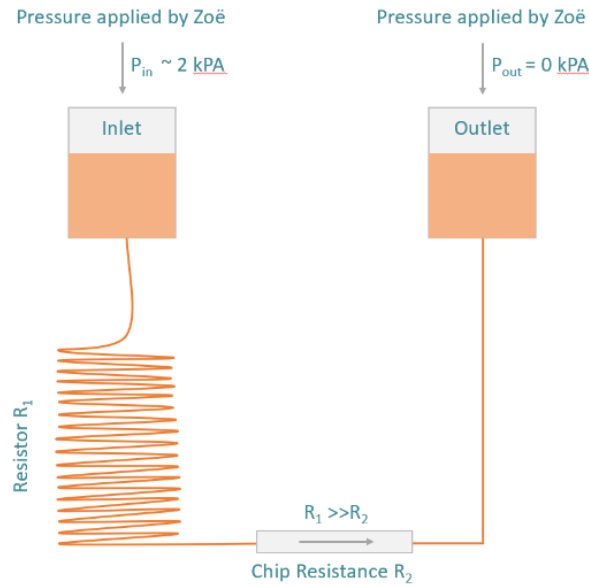


Figure 8 Schematic flow circuit for one channel

2.3 Chip Fabrication

Emulate Inc. provided the ready-to-use S1-Chip with 7 μm pore PDMS membrane, whereas the S1-Chip with 3 μm pore PET membrane and the Open Top Chip with 7 μm pore PDMS were fabricated by hand. The chip parts consist of a PDMS component containing the top channel, a PDMS component containing the bottom channel, and the respective membrane. The PDMS parts were replica molded as described previously[38], [68], by pouring PDMS (Sylgard, base: curing agent ratio is 10:1) into 3D printed molds (Fineline, USA) and overnight curing at 60°C. The 3 μm pore PET sheets (AR Brown, USA) were laser cut into rectangles with 2 mm diameter holes for the ports and the resulting membrane was cleaned from debris and plasma treated. After plasma oxidation, the membrane was functionalized with bis[3-(trimethoxysilyl)propyl]amine), washed in IPA, and rendered hydrophilic in 70% ethanol as previously described[69]. The functionalized membrane was bonded onto the plasma-treated PDMS chip parts aligning ports and channels under the microscope. The resulting dimensions are described in table 1. The PDMS components of the Open Top Chip were replica molded, and the 7 μm pore PDMS membrane was obtained using soft lithography. The parts were bonded using plasma treatment. After alignment under the microscope the channel ports were cleared of the membrane using tweezers. The gasket was 3D-printed in raisin.

2.4 Healthy primary airway epithelial cell culture

The workflow for healthy primary epithelial cells was optimized and the individual parts are explained in detail in the following sections. The general workflow is depicted in fig.7 and fig.8.

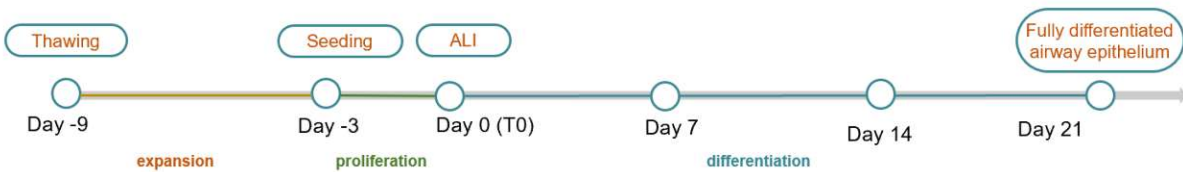


Figure 9 Basic Primary Airway Epithelial Culture. Primary cells are expanded in T75 flasks and harvested after 5 days. The cells are seeded onto the culture platforms and kept submerged for 3 days. Afterward, an air liquid interface is introduced to start the differentiation process that lasts for 21 days.

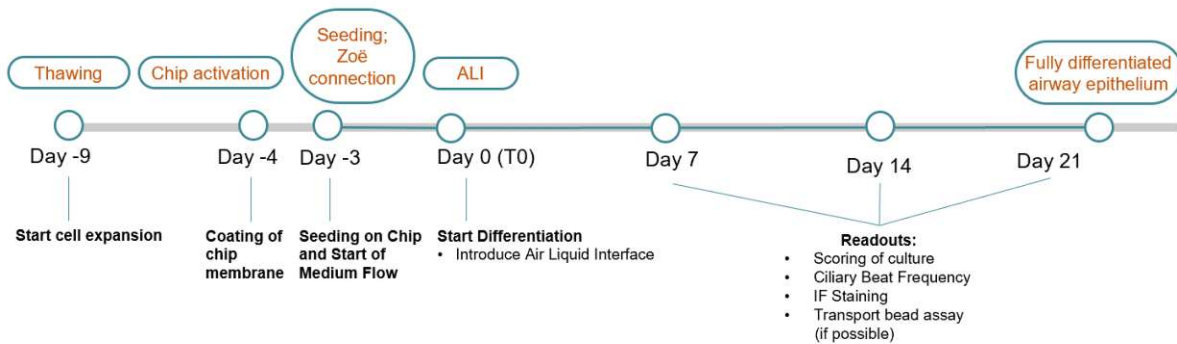


Figure 10 Timeline of Airway Chip culture. Before seeding cells onto the chip, the chip is activated by rendering membrane hydrophilic during the last day of expansion and coated with ECM. Cells are seeded onto the chip and the chips are connected to Zoë. After 3 days of medium perfusion in both channels, air liquid interface is established by introducing air to the top channel.

2.4.1 Cell Expansion

Primary normal human bronchial airway epithelial cells (PBECs) and primary normal human small airway epithelial cells (SAECs) were purchased from Lifeline® Cell Technology or were generously provided by the Department of Pulmonology of the Leiden University Medical Center. Cells were expanded in tissue culture-treated T75 flask in small airway epithelial cell growth medium (SAGM™ BulletKit™, Lonza) and Gentamycin from the SAGM SingleQuots™ supplements was replaced with 1% Penicillin-Streptomycin (Millipore Sigma). The medium was changed the day after seeding and then every other day. After five days (90 – 95% confluency), the cells were trypsinized and resuspended in serum-containing ALI medium (table 1) to stop trypsinization. The cells were centrifuged at 200 X g for 7 minutes at 24°C.

The cell pellet was diluted to a seeding density of 3,000,000 cells/mL for chip cultures and 300,000 cells/mL for static controls on transwell® (Corning Costar) plates. To optimize the cell culture condition for full epithelial cell differentiation on the S-1™ Chip, different medium conditions (table 1) were tested, and cells were diluted to desired seeding densities in respective media.

Table 2 Differentiation Media Composition

Medium	Reagent	Volume	Source	Cat. No.	
Complete PneumaCult™	PneumaCult™-ALI Basal medium	500 mL	StemCell Technologies	05001	
	PneumaCult™-ALI 10X Supplement		StemCell Technologies		
	PneumaCult™-ALI Maintenance Supplement	5 vials	StemCell Technologies		
		Heparin		StemCell Technologies	07980
		Hydrocortisone		StemCell Technologies	07925
		Penicillin-Streptomycin	5 mL	Sigma	P4333
Complete ALI Medium	Gibco DMEM/F-12	500 mL	Gibco	10565-018	
	KO serum replacement	5 mL	Lonza	10828010	
	Fetal bovine serum (FBS)	5 mL	Sigma	F4135 or F8317	
	Bulletkit supplements	Everything except Gentamycin, BSA, RA, EGF	Lonza	CC-4124	
		Penicillin-Streptomycin	5 mL	Sigma	P4333
Complete "Leiden" Medium	Gibco DMEM	500 mL	Gibco	10569-010	
	BEBM base	500 mL	Lonza	CC-3171	
	HEPES	12.5 mL of 1M solution in 500mL DMEM	Gibco	15630086	
	BSA	750 µL of 0.1% BSA solution per 500 ml medium bottle	Gibco	15260037	
		Bulletkit supplements	Everything except Gentamycin, BSA and RA	Lonza	CC-4124
		Penicillin-Streptomycin	5 mL per 500 mL medium bottle	Sigma	P4333

Complete “Leiden” 1/5 hEGF Medium	Gibco DMEM Glutamax	500 mL	Gibco	10569-010
	BEBM base	500 mL	Lonza	CC-3171
	HEPES	12.5 mL of 1M solution in 500mL DMEM	Gibco	15630080
	BSA	750 µL of 0.1% BSA solution per 500 ml medium bottle	Gibco	15260037
	Bulletkit supplements	Everything except Gentamycin, BSA and RA	Lonza	CC-4124
	Penicillin-Streptomycin	5 mL per 500 mL medium bottle	Sigma	P4333
	hEGF (Bulletkit supplements)	100 µL of EGF (<u>not all 500 µL</u>) per 500 ml medium bottle		
Mix 250 mL DMEM with 250 mL BEBM				

2.4.2 Transwell Controls

Cells were seeded at a density of 2344 cells/mm². Specifically, 200 µl of a cell suspension with 300,000 cells/mL, i.e., 75,000 cells total, was seeded onto 6.5 mm diameter tissue culture-treated transwell® inserts with 0.4 µm pore PET membranes. Media in the apical and basal compartments were refreshed the next day, and cells were kept submerged for 3 days to allow proliferation and the formation of a tight monolayer. Three days after seeding, air liquid interface (ALI) was introduced to start epithelial cell differentiation by aspirating the medium on the apical side and refreshing the medium in the bottom well (figure 7). Maintenance was performed every other day with an apical wash and media refreshment. Apical wash consisted of incubating the top well with warm Phosphate buffered saline (PBS) for 10 min and then aspirating it to remove accumulated mucus. Cell morphology was monitored during maintenance and on day 7, 14 and 21 of ALI.

2.4.3 S-1™ Chip cultures

The chip culture is sectioned into chip activation and coating, seeding, the connection of the chips to the pod, submerged culture phase and air liquid interface (fig 8).

2.4.3.1 CHIP ACTIVATION

PDMS is inherently hydrophobic but can be rendered hydrophilic by chemically activating the surface to allow the attachment of extracellular matrix proteins that provide an anchor for the cells to the microfluidic chip. This chemical activation was achieved by introducing a mixture of

proprietary compounds ER-1 and ER-2 (Emulate Inc.) at a concentration of 1 mg/mL into the channels, followed by exposure to UV light for 10 mins. After the UV treatment, the chips were washed twice with ER-2. This activation process was repeated once more. After the final washing step with ER-2, the chips were then filled with PBS (Sigma).

2.4.3.2 ECM COATING

To optimize epithelial cell adherence to the PDMS membrane, different extracellular matrices were tested.

For thin ECM coatings, the PBS in top and bottom channel was removed and replaced with an ECM solution (composition dependent on condition tested (table 3)). Specifically, the ECM proteins collagen IV (Col IV; collagen from human placenta, Millipore Sigma), collagen I (Col I; FibriCol, Advanced BioMatrix), fibronectin (Millipore Sigma) as well as bovine serum albumin (BSA) (7.5%, Gibco) were diluted in cold PBS at desired concentrations and immediately introduced into both channels of the chips. To ensure undisturbed settling of the ECM components onto the membrane for coating, the chips were incubated overnight at 37°C in a humidified petri dish.

To prepare 20-50 µm thick ECM gels (e.g., to generate a softer cell-substrate and prevent cell migration between channels), the PBS was removed only from the top channel and collagen I/IV hydrogels were introduced to the top channel. Collagen I/IV hydrogels were prepared using 0.5 mg/mL of collagen I and collagen IV in PBS. The hydrogel and the collagen components were kept on ice until introduction into the chip. PBS was retained in the bottom channel. Gels were incubated overnight at 37°C. The next day a gravity flush with PBS was performed by inserting an empty 200 µl filter tip into the top channel outlet port and a 200 µl filter tip filled with PBS kept at 37°C into the inlet port. Subsequently, the chip was flushed twice with warm PBS using an electronic pipette with 100ul at maximum speed and a pause interval of 5 sec.

Table 3 ECM conditions

ECM coating	Concentration
Col IV	300 µg/mL
Col I + Col IV	100 µg/mL + 300 µg/mL
	300 µg/mL + 100 µg/mL
Col I + BSA	300 µg/mL + 0.1 mg/mL
Col I + Fibronectin + BSA	100 µg/mL + 50 µg/mL + 0.1 mg/mL
	300 µg/mL + 16.66 µg/mL + 0.1 mg/mL
BSA	0.1 mg/mL
Col I + Col IV Gel	0.5 mg/mL + 200 µg/mL
Col IV Gel	1 mg/mL
Col IV + Matrigel Gel	400 µg/mL col-IV + 200 µg/mL Matrigel

2.4.3.3 SEEDING

Before seeding, the bottom channel of the chips was filled with a cell culture medium and placed into the incubator to equilibrate the medium. The cells were diluted to a suspension of 3,000,000 cells/mL resulting in a seeding density of 3000 cells/mm² and carefully seeded to the top channel via the top channel inlet port. The chips were quickly inspected under the microscope to confirm a homogeneous distribution of cells and placed into the incubator for 4 hours to allow the cells to settle and adhere. After 4 hours, the top and bottom channels were gently washed with fresh medium to remove non-adherent cells and debris and placed back into the incubator for another 2 hours before connecting the chip to the Pods and subsequently to the Zoë.

2.4.3.4 CONNECTION TO POD

Steriflip® filters (Millipore) were used to de-gas media by attaching the filter units to 50 mL Falcon tubes containing warm medium and connecting to vacuum pumps. A vacuum was applied for 15 min to eliminate excess gas from the medium and prevent bubbles from being formed and trapped in the chip. After 15 minutes, the assembly was disconnected from the vacuum pump and medium supplemented with retinoic acid (Millipore Sigma) or EC-23 (Torcis). 3 mL of medium were transferred into the top and bottom inlet reservoir of the Pod and 300 µl of medium were placed into the top and bottom outlet reservoir. The Pods were placed into Zoë and the "prime" cycle was selected. The "prime cycle" applies pressure to both inlet and outlet reservoirs resulting in the flow of medium into the manifolds and out through the Pod ports, as evidenced by the formation of medium droplets on the Pod ports. These droplets are desired to ensure a liquid bridge is formed between the ports of the Pod and the ports of the chips upon connection. To further ensure liquid bridging, droplets were also placed on all ports of the chip before contact. Chips were then connected to the Pods using the plastic clamp built into the Pod. After connection, a "via wash" was performed by pipetting the medium just above the ports referred to as vias (for distinction from chip ports) of the reservoirs and releasing it on the wall of the Pod. This removes any potential air bubbles blocking the via and preventing medium flow into and out of the chips.

2.4.3.5 CONNECTION TO ZOË

After the via wash, the chip containing Pods were placed into the Zoë using the two Zoë trays. Each Zoë can maintain a total of 12 chips, with 6 chips per tray. The volumetric flow rates of the top and bottom channels were set to 30 µL/h and the "regulate cycle" was selected. The regulate cycle takes two hours and pressurizes the inlet and outlet reservoirs to increase the concentration of gas that the liquid can dissolve, leading to the reduction and solving of air bubbles that may be present and could not be dislodged manually or that are not visible by eye. After the regulate cycle, Zoë automatically switches to regular perfusion of the chips with medium using the indicated volumetric flow rates.

2.4.3.6 SUBMERGED PHASE

One day after connection, another via wash was performed, and the regulate cycle was selected again. The medium was changed the day after, and the waste medium collected in the outlet reservoirs was aspirated.

2.4.3.7 AIR LIQUID INTERFACE

Air liquid interface was introduced 3 days after seeding. For this purpose, the medium was removed entirely from the top channel reservoirs and the bottom outlet reservoir. The chips were placed back to Zoë, and the top and bottom channel volumetric flow rates were set to 1000 $\mu\text{L}/\text{h}$ and connected for roughly 1 minute, thereby introducing air into the top channel. The medium removed from the top channel was aspirated, and a medium plug of 1 mL was added to the top in- and outlet reservoirs. The medium plug is used to counteract the hydrostatic pressure increase over time resulting from the collection of waste medium in the bottom channel outlet reservoir. Unless counterbalanced, the waste-mediated pressure acts on the bottom channel and filtrates fluid into the top channel, which can be harmful to the cells and submerge the air liquid interface, creating edema-like conditions. In addition, the medium plug prevents continuous evaporation from the top channel and hence ensures a humidified environment for the airway cells.

2.4.3.8 MAINTENANCE

The medium was changed every other day in the bottom inlet reservoir as well as in the top inlet and outlet reservoir that form the plugs. After each medium exchange, a via wash was performed. An apical wash for removing accumulating mucus was performed twice a week. First, the medium plugs and the waste built up in the bottom outlet reservoir were aspirated, and 300 μL of warm PBS was added into the top inlet reservoir above the via. Next, the flow rates of the Zoë were set to 1000 $\mu\text{L}/\text{h}$ for both channels, and flow was introduced for an average of 2 mins until the top channel was submerged in PBS. Then, the cells were incubated for 10 to 30 minutes in the submerged state to dissolve the mucus. During this incubation time, the cells' morphology was monitored and assessed using phase-contrast microscopy, as the cells are best visible when submerged. ALI was reintroduced by aspirating the PBS from the top inlet reservoir and flowing at 1000 $\mu\text{L}/\text{h}$ (both channels) for roughly 1 minute. The PBS in the outlet reservoirs was removed, and the top channel reservoirs were sealed with 1 mL medium. Cell morphology was monitored on 7, 14 and 21 days of ALI to check viability and function (ciliary beat).

2.5 Cystic Fibrosis airway epithelial cell culture

2.5.1 Cell Expansion

Diseased primary human bronchial tracheal airway epithelial cells (BTECs) from donors carrying mutations in the CFTR protein that cause cystic fibrosis were purchased from different vendors and tested for cell culture. A detailed list of the vendors, the genetic background of donors, and

donor information can be found in table 4. Cells were expanded as described above for healthy cultures, the only difference being that the duration of expansion to reach ~90% confluency ranged from 4 to 16 days depending on the cell source.

Table 4 Donor List Cystic Fibrosis

Donor	Mutation	Vendor	Age	Gender	Ethnicity	Alcohol	Smoking	Medication	Additional Comments
FC-0103	Cystic Fibrosis homozygous F508del	Lifeline	20	F	C			n/a	Cause of Death: Anoxia
16756	Cystic Fibrosis homozygous F508del	BioIVT	25	F	C	N	N	Omeprazole, Azithromycin, Colomycin, Tiotropium, Salmeterol, Salbutamol	Cystic Fibrosis, Osteoporosis, Sinusitis
450918	homozygous deletion c.1521_1523 delCTT del508 in exon 11, homozygous missense mutation c.1408G>A (p.V470M) in exon 11	Lonza	25	M		Y	N	O2, Azithromycin, Sulfamethoxazole, vanomycin, flonase, cyproheptadine, pulmozyme, symbicort, ventolin, ergocalciferol, ferrous sulfate, hypersal 7%, pantoprazole, viokace, zenpap	n/a
222158	p.V470M heterozygous variant in Exon 11, p.508del heterozygous in exon11, p.L558S heterozygous variant in exon12	Lonza	28	F	C	N	N	Zyvox	Diagnosed through a sweat test, patient admitted with shortness of breath

2.5.2 ECM coating

To optimize cell culture conditions, different ECMs were tested. Transwell inserts were coated with 300 µg/mL collagen IV in PBS overnight at 37°C one day before seeding according to the standard CF *in vitro* protocols for transwell cultures[70]. The coating solution was removed right before cell seeding. Collagen I gels were prepared at different concentrations (8 mg/ml, 5 mg/mL and 3 mg/mL) over ice by diluting collagen I in reconstitution buffer (1.2 g sodium bicarbonate and 3.06 g HEPES in 75 mL of 0.067 M NaOH) and adjusting the pH with 1N NaOH to a neutral pH where necessary. 50 µL of collagen I gel was introduced to the transwell insert. In another approach, gels were molded to a height of 50 µm using a sterilized ring-shaped spacer and PDMS stamps cut out with a 6 mm biopsy punch (Stiefel). After placing the spacer into the transwell, the freshly prepared ECM solution was added. Then, the stamp was placed on top of the spacer, limiting ECM gel formation to the space enclosed by the bottom of the insert, the circular opening of the spacer ring, and the stamp surface, hence creating a defined gel height as well as an even surface. The gels were placed into an incubator at 37°C overnight and then coated with 300 µg/mL collagen IV (as described above) for 4 hours. The collagen solution was removed prior to seeding.

10% gelatin gel was prepared two days before seeding over ice, and 4% microbial transglutaminase (Modernist Pantry) was used to additionally crosslink the gelatin gel by forming isopeptide bonds between the proteins. The gels were stamped down using the same approach as described above. After overnight incubation at room temperature, the gels were hydrated and functionalized with collagen IV using NHS-EDC crosslinking. Here, 0.4mg/mL EDC (Thermo Fisher Scientific) in sodium acetate buffer was mixed with 1.1 mg/mL NHS (Sigma) in sodium acetate buffer and 1 mg/mL collagen IV. The mix was diluted 20 times in PBS, placed over the gelatin gel, and incubated overnight at 4°C.

2.5.3 Transwell culture

Cells were seeded at a density of 400,000 cells/mL, that is, 100,000 cells per insert, onto 6.5 mm tissue culture-treated transwell® inserts with 0.4 µm pore PET membranes or polycarbonate membranes for increased stiffness and maintained as described above (see: Transwell Controls). The CF cultures were kept submerged for 3 days to 10 days depending on the culture conditions and cell source until they formed a monolayer or almost complete monolayer.

2.5.4 Chip cultures

Three chip types were tested for the CF on-chip culture. Healthy PBECs or SAECs were used as control. The three chip types that were potential platforms candidates included a 7µm pore PET membrane chip in S1 architecture, the Open Top Chip that has an easy-accessible chamber connected to the top channel, and the S-1™ Chip with a 4 µm pore PDMS membrane.

2.5.5 Open Top Chip Culture

Before coating, the chamber's surface and bottom channel were activated as described in section 2.4.3. The second treatment was performed to minimize failed surface activation. After removing PBS from the chamber, the OT chips were coated with either 8 mg/mL or 3 mg/mL collagen I gel (gels were prepared as described above). The gels were stamped down to a height of 200 µm using a 3D printed stamp (printed through Protolabs) that is supported by a rectangular frame resting on the top surface of the chip while the body of the stamp protrudes into the chamber, leaving room for the excess gel to evacuate the chamber. The chips were placed into a petri dish containing PBS reservoirs, and the dishes were sealed and incubated at 37°C overnight. The stamps were carefully removed the next day, avoiding damage or removal of the gel, and coated with 300 mg/mL collagen IV for 4 hours. The coating solution was removed, and cells were seeded at a density of 3000 cells/mm². The cells were kept static in the submerged phase until the formation of a monolayer or an almost complete monolayer formation was observed (3 to 10 days).

2.5.5.1 CONNECTION OF OPEN TOP CHIPS TO PUMP AT ALI

Since the Open Top Chip is still under development and Zoë compatibility has not been determined, the OT chip was instead perfused using a multichannel peristaltic pump (IPC 16, ISMATEC) via PharMed® BPT 0.25mm tubing (ISMATEC). Therefore, the OT chip was placed into a plastic gasket containing the top channel. The medium in the chamber was aspirated manually using a pipette to introduce ALI. The bottom channel was connected via PharMed® BPT 0.89 mm Tubing (Cole-Parmer) to the medium reservoir and via PharMed® BPT 0.25mm tubing to the pump and ultimately to the medium waste reservoir. The top channel was connected to 5 cm PharMed® BPT 0.89 mm tubing and closed off for sterility. The flow rate was set to 0.01 mL/min, the tubing was primed with medium, and the flow was started. Cells were monitored and maintained daily. Apical washes were not performed as cell cultures did not survive far enough into the differentiation process (see results).

2.5.6 S1-Chip culture

The cystic fibrosis cell culture on the chip followed the timeline of the healthy culture and underwent the same culturing steps. The activated chips were coated with either 0.3 mg/mL collagen IV or 0.5 mg/mL collagen I/IV hydrogels determined optimal in healthy S1 culture and transwells. Different differentiation media previously tested in transwells were used.

Table 5 Media Conditions for CF Culture

Differentiation Media (ref. table 2)
Complete PneumaCult™
Complete ALI Medium
Complete “Leiden” Medium
Complete “Leiden” 1/5 hEGF Medium
Complete “Leiden” 1/5 hEGF Medium + 4% Serum (2% HyClone + 2% KO Serum Replacement)
Complete “Leiden” 1/5 hEGF Medium + 2% Serum (2% KO Serum Replacement)

2.6 Immunofluorescence Staining

Immunofluorescence staining was performed on chips and on transwells. For this purpose, samples were washed twice with PBS and fixed with 4% paraformaldehyde (Electron Microscopy Sciences) for 20 minutes. Subsequently, all samples were washed twice with PBS and incubated with a blocking buffer composed of 0.5% Triton x100 in 5% BSA in PBS for one hour at 4°C. After incubation, the samples were washed once in PBS (5 min). Chip samples were cut into three segments with a razor blade. The samples were then incubated with mixtures of the following primary antibodies: mouse monoclonal Muc5AC (Lab Vision™, Thermo Fisher Scientific, MS-145-P1, 1:500), directly conjugated monoclonal alpha-tubulin (Abcam, Alexa Fluor® 594, ab202272, 1:100), rabbit monoclonal p63 (Abcam, ab124762, 1:100), mouse monoclonal CC16 (Hycult Biotech, HM2178, 1:50), mouse monoclonal ZO-1 (Invitrogen, 33-9100, 1:100), directly conjugated monoclonal ZO-1 (Invitrogen, Alexa Fluor® 594, 339194, 1:200) and mouse monoclonal CFTR C-Terminus (R&D Systems, MAB25031, 1:100). The primary antibodies were diluted in blocking buffer in varying combinations, and samples were incubated with the antibody mixes at 4°C overnight. After incubation, samples were washed with PBS three times for 5

minutes each. The last wash was followed by incubating the samples with mixes of the following secondary antibodies in blocking buffer: AlexaFluor® Plus 647 donkey anti-rabbit IgG (Invitrogen, 1:200) and AlexaFluor® Plus 488 goat anti-mouse IgG (Invitrogen, 1:200). Additionally, the samples were stained with DAPI (Abcam, ab228549, 1:200) and phalloidin 647 (Invitrogen, A22287, 1:200). The samples were incubated with secondary antibodies, DAPI and phalloidin for one hour at room temperature and then washed with PBS three times for 5 minutes. Prolong Glass Antifade Mountant (Invitrogen) was used to mount cut-out transwell membranes onto glass slides in some cases or introduced into the exposed channels of the chip parts.

2.7 Lactate Dehydrogenase Cytotoxicity Assay

Lactate dehydrogenase (LDH) levels of effluent media were measured as a qualitative measure to observe the trend of LDH quantity, e.g., cell death within one experiment, as the variability of results between LDH kits is high. The kit used was the CytoTox 96® NonRadioactive Cytotoxicity Assay (Promega). Medium in the outlet reservoir was removed on the morning of the day of interest, and effluent medium samples were taken after 24 hours of flow from the outlet reservoir. A positive control of LDH in PBS and negative controls for the respective medium conditions were prepared. LDH levels for effluent media were measured in duplicate. In this coupled enzymatic assay, tetrazolium salt is converted into a red formazan product. The absorbance of the red formazan product was measured using the BioTek™ Synergy™ NEO HTS Multi-Mode Microplate Reader. The absorbance was plotted in histograms to compare LDH levels indirectly. In some cases, absorbance was corrected for the negative control value and plotted as the percentage of the absorbance of the positive control.

2.8 High-Speed Video Microscopy

High-speed videos of ciliary beat and fluorescent microbead transport were taken using the Zeiss Z1 AxioObserver inverted microscope equipped with a Pecon chamber for temperature control for live imaging and an ORCA-Flash4.0 V2 high-speed camera. Before live imaging, an apical wash was performed to remove mucus as described earlier, and the Pecon chamber was heated to 37°C.

2.9 Cilia Imaging

Cell cultures on transwells and chips were placed onto the microscope stage. The condenser diaphragm was adjusted to achieve optimal Koehler illumination of the ciliated surface at a

magnification of 40x. Further, the turret rotation thumbwheel was set to a position between condenser annulus H and the condenser annulus PH1 to achieve oblique illumination and hence increased contrast. The microscope was controlled via the Zeiss Zen software. The following settings were selected prior to recording: 1024 x 1024 pixels ROI, 2x2 binning, 2s recording time, exposure time 1.004 ms, resulting in a final movie frame rate of approximately 200 frames per second. Three to six movies were taken per sample on different representative areas.

2.10 Bead Transport

In order to measure mucociliary clearance, 1 μm polystyrene microspheres (FluoSpheres™, Invitrogen, red fluorescent 580/605) were diluted in warm SAGM (37°C) at a ratio of 1:1000 and, following an apical wash, the solution was transferred into the chip or onto transwell inserts. The sample was placed onto the microscope stage, and the condenser was adjusted at a magnification of 10x. Following settings were selected in Zeiss Zen prior to recording: 1024x1024 pixels ROI, 2x2 binning, 13s recording time, 40ms exposure time. Three movies were taken per sample.

2.11 Image Analysis

Images were analyzed using Fiji[71] and MATLAB (MathWorks). The bead movies were analyzed using the TrackMate Plugin[72] in ImageJ.

3 Results

3.1 Emulating the Healthy Human Airway

The basis for chip culture optimization was the protocol for small-airway-on-a-chip described by Benam et al.[38] and further developed internally at Emulate Inc. for organ chips with PET membranes. In this work, these protocols for Emulate's S-1 Chip with a PDMS membrane were validated in order to assess whether processes can be continued on the new culture platform or if they had to be adopted. Considering the complex nature of dynamic organ-on-a-chip cultures, several biological and mechanical parameters had to be optimized. To evaluate different parameter conditions and to be able to terminate long-term culture early if a condition was not promising, a standardized visual quality control was introduced. We quantified six differentiation and cell viability markers in this quality control and scored the cultures under investigation on a scale from 0 (excellent) to 3 (poor). The markers are cell death, ciliation, attachment of cells to the membrane, shape and movement (deviation from cobblestone morphology towards aligned and elongated cells) of the cells, overgrowth, and invasion of epithelial cells in the top channel towards the other side of the membrane. Color coding (green 0 to red 3) of the final score and the rendering of heatmaps for cultures (attachment 1) allowed for a straightforward assessment of promising culture conditions.

The healthy airway culture was optimized for the Emulate S-1 Chip hosting a PDMS membrane. In order to grow cells on PDMS covered with ECM, the hydrophobic membrane has to be functionalized. Hence, the activation process of the membrane had to be adapted. The aim was to establish ubiquitous adherence of ER-2, the linker molecule that binds to the PDMS surface, and specifically the prevention of bubble formation within the ER-2 solution during UV treatment. Therefore, the common activation protocol provided by Emulate Inc. was altered so that UV treatment was split in two times 10 minutes instead of 20 minutes and repeated introduction of ER-2 in between UV treatment to saturate the chip with linker molecules. This resulted in the absence of bubble formation and homogenous color change of ER-2 after UV treatment throughout all chips.

Next, the extracellular matrix providing spots of adhesion for the cells underwent optimization (fig 9). Different ECM compositions and concentrations were tested as described in table 3. All ECM solutions had a pH of 7. When comparing conditions with lower collagen I concentrations and collagen IV only, all conditions had stretched and stressed cells, showed holes within the cell layer, patches of enlarged cells, as well as overgrowth, and cases of epithelial-mesenchymal

transition (EMT) were large amounts of fibroblasts appeared. The response of the cell cultures within each condition was highly variable and therefore not comparable to each other. Most cell death was observed in collagen I/IV coating. In another round of experiments with increased collagen I concentration and BSA only, all conditions showed overgrowth and invasion, but this time, all chips within one condition exhibited similar characteristics (attachment 2). Although minor holes in the cell layer were observed after seeding in chips with BSA coating only, almost no holes were visible the next day, and they eventually closed. After 14 days of ALI, cilia were observed under a phase-contrast microscope on BSA coated chips after washing, indicating proper differentiation.

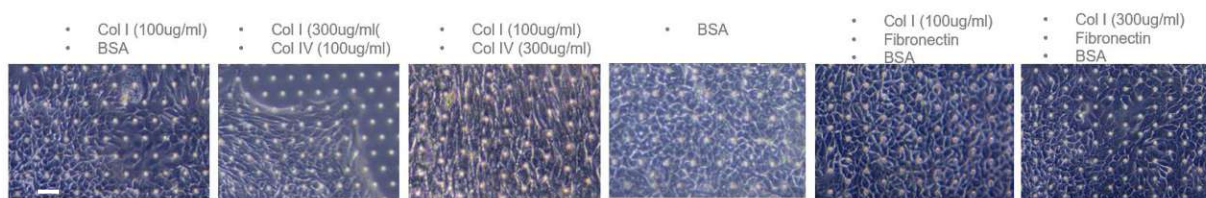
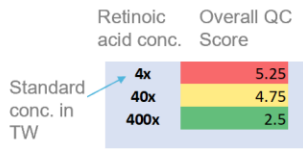


Figure 11 ECM conditions. The primary airway epithelial cells reacted drastically differently to each ECM condition. Best results were observed with BSA coating, and worst results were obtained using collagen I and collagen IV, as seen in the representative phase-contrast images. Where BSA shows cobblestone morphology and collagen I/IV either detaches or shows EMT.

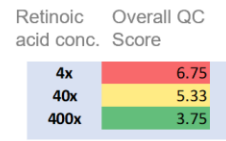
To tackle overgrowth, invasion and movement, we tested different medium conditions as described in section 2.4. The ECM conditions were tested in either complete ALI medium or complete Leiden medium. Cells cultured in ALI medium detached from the membrane and displayed patches of stretched, flat and enlarged cells. Leiden medium showed good cell morphology, but the chips were heavily overgrown and several cell layers formed on top of each other. To tackle this problem, human epithelial growth factor (hEGF) was reduced by 80%, a supplement of Leiden medium. There were no holes visible in the cell layer after seeding, and the cell layer remained integer for 14 days after exposure to ALI.

Nevertheless, these chips showed low to no ciliation and invaded cells in the bottom channel. Supplementing Leiden medium with serum and excluding hEGF resulted in decent ciliation but a detachment of cells after 10 days of ALI. To approach complete differentiation, titration of retinoic acid concentration was performed, with the results showing that a 100-fold increase of retinoic acid improves the differentiation state of the cell culture (fig 10). This complies with the material properties of PDMS, as it has been found that PDMS can adsorb hydrophobic and negatively charged molecules[73].

a) 7 days on ALI



b) 14 days on ALI



Detailed Breakdown of QC Scoring

	Ciliation	Attachment/peeling	Movement	Over-growth	Invasion	Cell death
4x	2.25	0.5	0.75	1	0.75	0
40x	2	0	0.25	1	1	0.5
400x	1.25	0	0	0.75	0.5	0

Detailed Breakdown of QC Scoring

	Ciliation	Attac-peelin	Move-ment	Over-growth	Invasion	Cell death
4x	2.3	1.0	0.0	0.0	2.0	1.5
40x	1.7	0.7	0.3	0.0	2.0	0.7
400x	1.5	0.0	0.0	0.0	2.0	0.3

(4 chips/condition)

c)

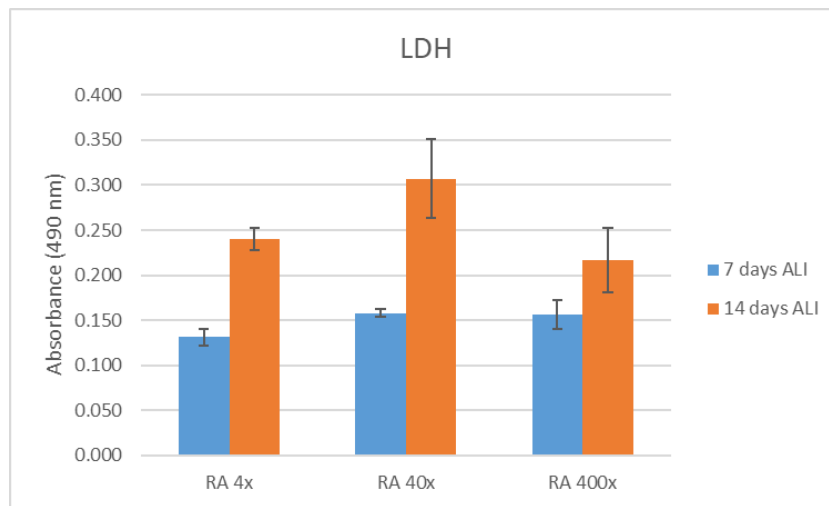


Figure 12 A 100-fold higher retinoic acid concentration than in regular transwell cultures improves cell viability and differentiation. Both at a) 7 days and b) 14 days on ALI the 100-fold higher concentration shows the best quality control ranking. c) This is also confirmed by LDH photometry on day 14.

Other media conditions tested (fig 11, 12) had D-valine DMEM/F-12 as base medium and Leiden Medium or ALI medium supplements to prevent fibroblast proliferation that could be observed in some chips and might result from EMT[74]. Cells in the medium condition D-valine DMEM/F12 plus ALI medium supplements died after 7 days, so did cells in DMEM and Leiden aliquots in the same set of experiments. D-Valine DMEM/F12 and BEBM base medium mixed at a ratio of 1:1 plus Leiden supplements showed decent ciliation and cobblestone cell shape. Still, the chips were invaded and eventually detached in some regions. The epithelium in PneumaCult medium was heavily overgrown, but after 14 days on ALI most of the cells in the top layers died, and a fully ciliated monolayer appeared. At first, no invasion was observed in the chip, but after more than 7 days of culture, cells start to appear on the other side of the membrane and throughout the bottom channel. The 50% dilution of complete PneumaCult medium with PneumaCult-ALI basal medium

yielded similar results but convinced with high ciliation, no movement of the epithelium, minor overgrowth as compared to 100% complete PneumaCult and almost no cell death. Both PneumaCult medium conditions enabled complete differentiation at 3 weeks of ALI, in terms of ciliation and mucus production. However, overgrowth at the start of culture and invasion was not resolved.

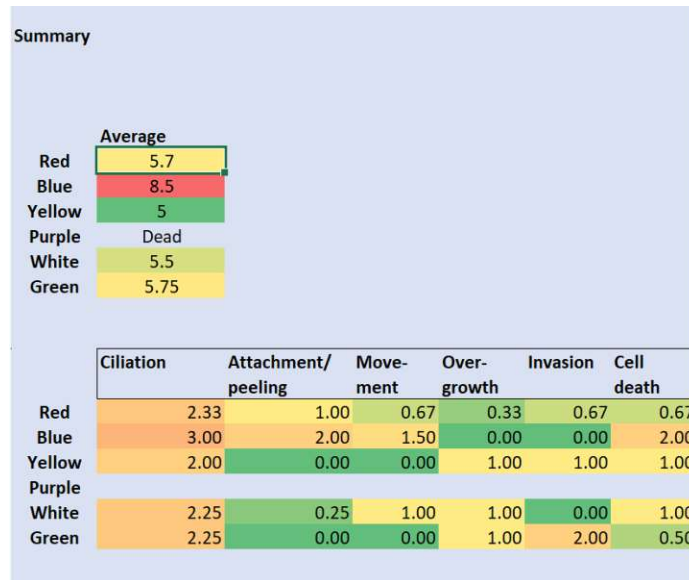


Figure 13 Scores 7 days after Introduction of ALI for several medium conditions tested in one experiment with 4 chips per condition. Conditions – red: ALI medium; blue: DMEM/HEPES + Leiden supplements; yellow: D-valine DMEM/F12/BEBM (1:1) + Leiden supplements; purple: D-valine DMEM/F12 + ALI supplements; white: PneumaCult ALI; green: Leiden 1/5 hEGF + Y-compound

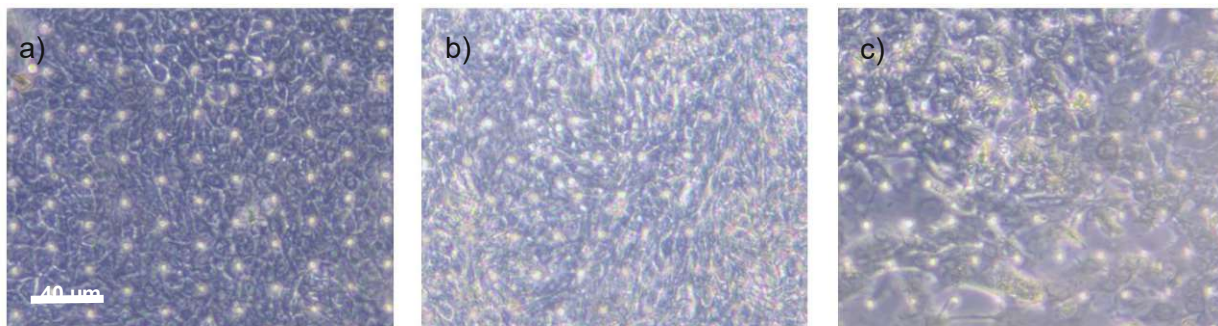


Figure 14 phase-contrast images of cells grown in a) D-valine Leiden b) PneumaCult c) ALI medium

To stop cells from invading the bottom channel, the introduction of gel into the top channel was tested to block the pores of the membrane. Thus, three different gel conditions were tested, collagen IV gel, collagen I/IV gel and collagen I/Matrigel, for their effect on invasion but also cell morphology, differentiation and viability. Collagen IV gels did not cover the top channel's entire surface, and most of the gel was removed when flushing the channel with medium (attachment

3). Nevertheless, gels do minimize the migration of cells into the bottom channel (attachment 4). Out of eleven chips, only one chip was fully invaded in collagen I/Matrigel gels after 14 days of air liquid interface. In chips containing collagen IV gels, no chip was fully invaded at 14 days of ALI. Still, sparse distribution of epithelial cells on the other side of the membrane could be observed already after 3 days on ALI. One out of four chips was fully invaded in collagen I plus collagen IV gel containing chips at 14 days of ALI, and in control chips only coated with 0.1% BSA, six out of eight chips displayed heavy invasion. Due to recurrent failure of the instrumentation and submersion of the cells, it is not clear whether the presence of invasion and worsening of cell morphology in all conditions, observed on day 14, is due to the cells reaction to the gel substrates or rather (and more likely) wound healing processes that are triggered after repeated submersion of cells and exposure to pressure spikes and static periods of up to 10 min. Staining of the cells grown collagen I/IV gels and on collagen I/Matrigel gels revealed the presence of all major cell types of the airway epithelium (fig 13).

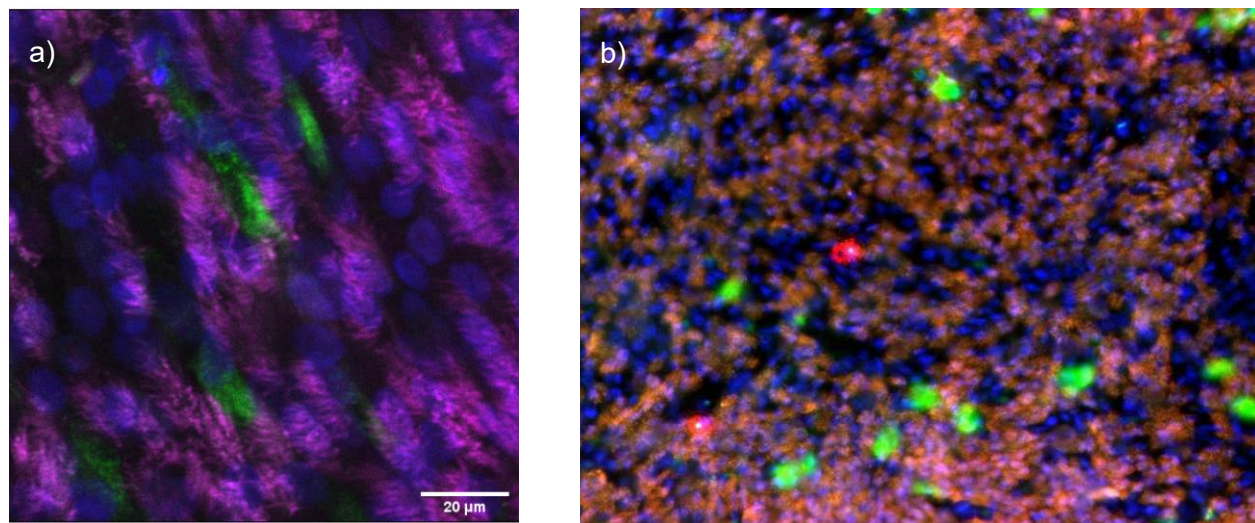


Figure 15 Staining of healthy culture growing on collagen I/IV gel in the S1-Chip; a) cell nuclei in blue (DAPI), goblet cells in green (Muc5AC), ciliated cells in magenta (alpha-tubulin); b) cell nuclei in blue (DAPI), goblet cells in green (Muc5AC), ciliated cells in orange (alpha-tubulin); club cells in red (CC16)

The functioning of the mucociliary escalator could be shown by bead assay and motion tracking of the beads on the airway epithelium in all chips at 25 days of ALI (fig 14). The streamlines of beads could be visualized and showed local alignment. Motion detection of cilia beating revealed a dense distribution of cilia.

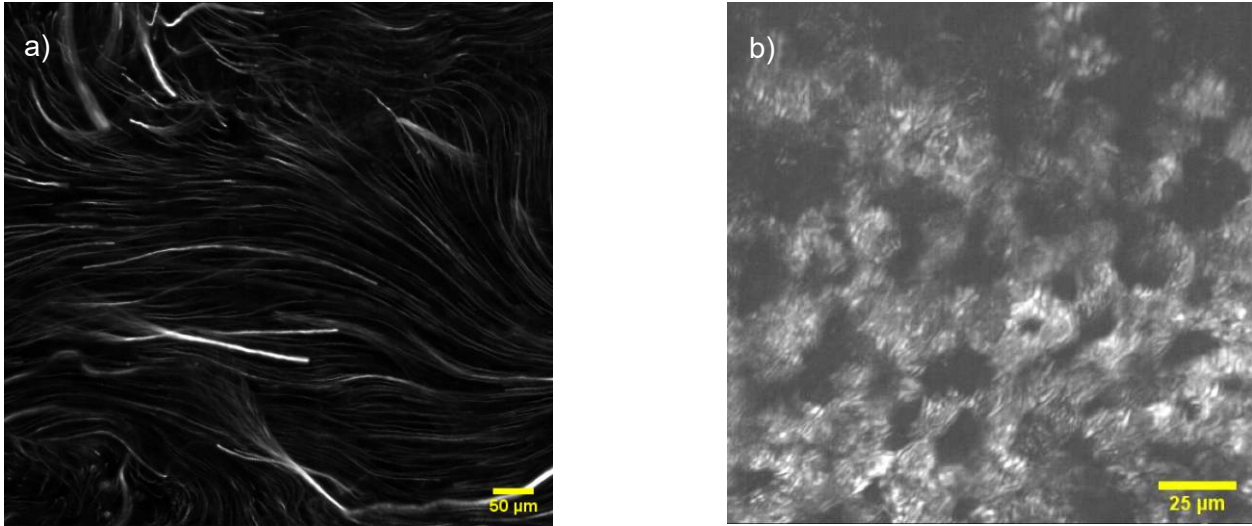


Figure 16 Motion detection revealed a) a functioning mucociliary escalator and b) cilia beating and high cilia coverage. Further, the onset of flow was adapted. It was tested whether a later start of perfusion can improve epithelial cell viability and whether a higher flow rate can improve differentiation and viability. Therefore, the PET membrane-based protocol where flow is started 2 hours after seeding was compared to flow onset 6 hours after seeding. Keeping the culture static for 6 hours with a refreshment of media 4 hours after seeding improved cell viability (fig 15).

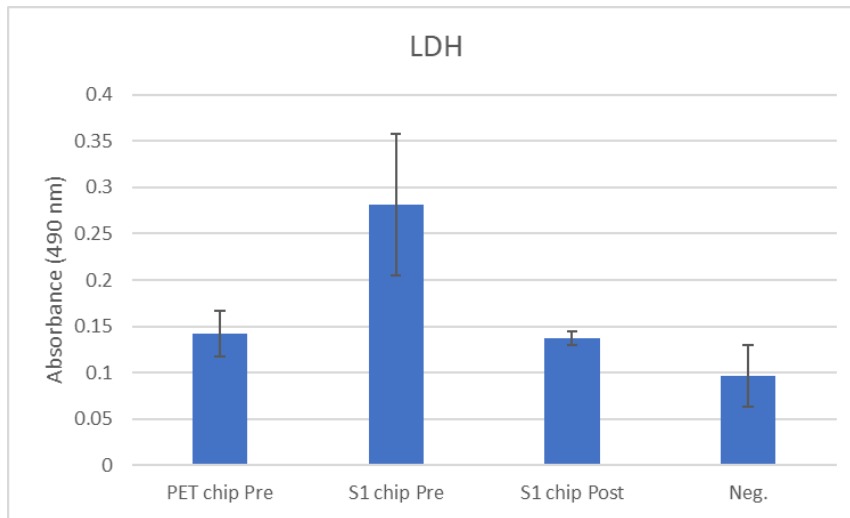


Figure 17 LDH levels of effluent - PRE = flow onset 2 hours after seeding; Post = flow onset 6 hours after seeding and refreshment of medium after 4 hours

As already mentioned, primary airway cultures are grown at air liquid interface, which can be achieved in the chip by removing the medium from the top channel and perfusing the bottom channel with media. In a closed automated system where cells are grown on porous membranes, the risk of evaporation has to be eliminated, and hydrostatic pressures have to be balanced. The

accumulation of effluent medium in the bottom channel outlet reservoirs of the Pod through perfusion leads to an increased hydrostatic pressure that pushes against the membrane. The pressure eventually reaches a hydrostatic head that causes the flooding of the top channel and the disruption of the cell layer. To counteract the pressure, different medium plugs for the top channel in- and outlet reservoirs were tested. Starting with 200 μL according to the provided protocols, 1 mL plugs modeled based on the assumption of equal surface area of the inlet and outlet reservoirs (fig 16) were tested and computed values of 1.88 mL and 1.91 mL based on the actual surface areas measured using CAD. Additionally, in one condition, the top channel reservoirs were plugged with 1 mL of medium, and the outlet reservoir of the bottom channel was emptied every day to create a higher hydrostatic pressure in the top channel at all times.

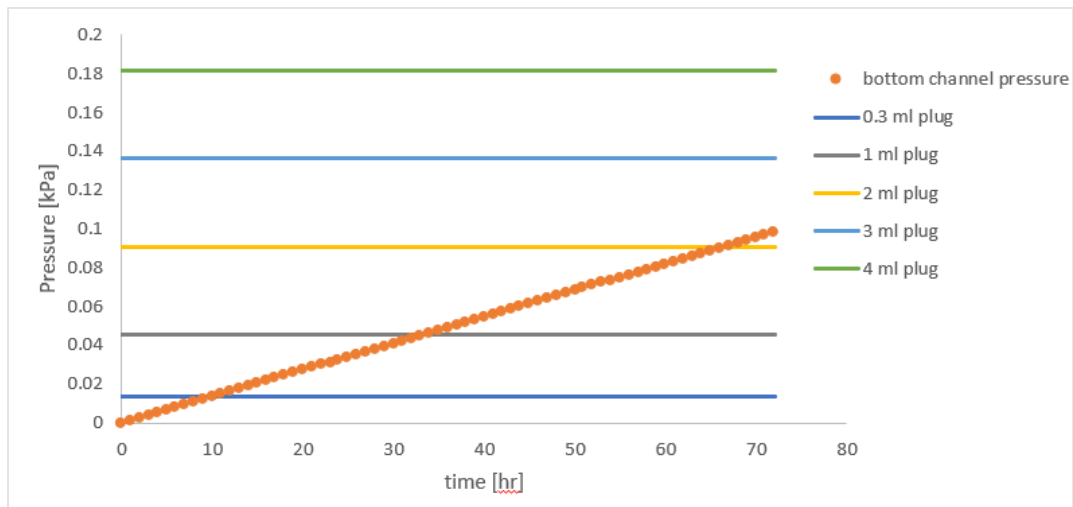


Figure 18 Comparison of pressures in top and bottom channel. A 1 mL medium plug in the top channel reservoirs balances the pressure due to the waste building up in the reservoirs for up to 32h. Empirically, up to 72h of continuous perfusion (and waste buildup) was supported with this protocol, likely because the cellular barrier function adds sufficient resistance to withstand the pressure differential up to this point.

Air liquid interface could not be maintained throughout a culture period of 14 days with 200 μL plugs. The condition with the lowest (and therefore best) average quality control score at 7 and 14 days of ALI was the condition using the exact surface areas. Yet, the condition using 1 mL medium plugs without daily removal of effluent medium convinced because of more favorable culturing processes relative to gain. The scores of the individual cell differentiation and viability markers were only slightly elevated apart from one outlier, where cells detached from the membrane, raising the average score (fig 17).

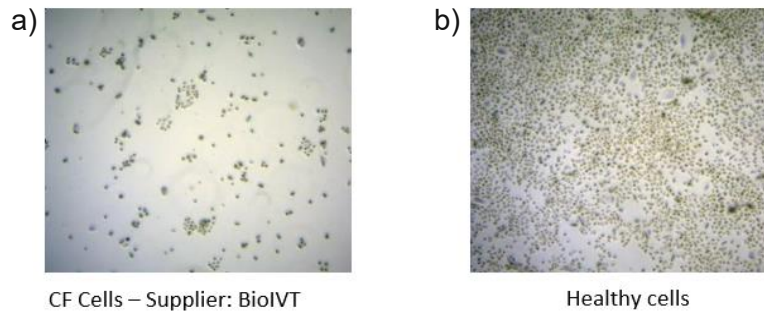


Figure 19 Average score for each pressure condition on 14 days of ALI (N=4 chips). Pressure experiments were performed in Leiden 1/5 hEGF. Conditions, A: 1.88 mL (inlet plug) and 1.91 mL (outlet reservoir) plug; B: 1 mL plug and daily waste removal; C: 1 mL plug; D: 200 μ L plug; E: 1 mL plug in 1:1 Leiden 1/5 hEGF medium and Leiden 1/5 hEGF conditioned in transwell culture of same the same donor. See attachment 5

3.2 Emulating the Cystic Fibrosis Airway

Before chip culture, successful cell sources and culture conditions had to be determined as diseased primary cells are demanding and difficult and sometimes even impossible to culture due to their reduced robustness. And hence all optimization processes were performed in transwells to minimize cost, time and culture complexity. The basis for cell culture optimization was the protocol described by Randell et al.[70], the protocol for healthy airway cultures provided by Emulate Inc., and the acquired knowledge from the optimization studies of the healthy airway. Several sources of primary human cystic fibrosis bronchial/tracheal epithelial cells had to be tested for the model development. Differences in cell sources included the detachment of cells from the membrane and extended cell expansion periods until ~90% confluency of 12 days compared to 5 days expansion for other CF cell supplies and healthy controls (fig 18). All donors were tested on collagen IV coated transwells and cultured in both Leiden and ALI medium. Successful cell sources were donor 450918 from Lonza and FC-0103 from lifeline (see table 4). Cells of these donors remained attached to the membrane of transwell inserts and differentiated showing ciliary beating and mucus secretion.

Example of confluency of plated cells after 5 days



Attachment of cells on transwells after 7 days on ALI

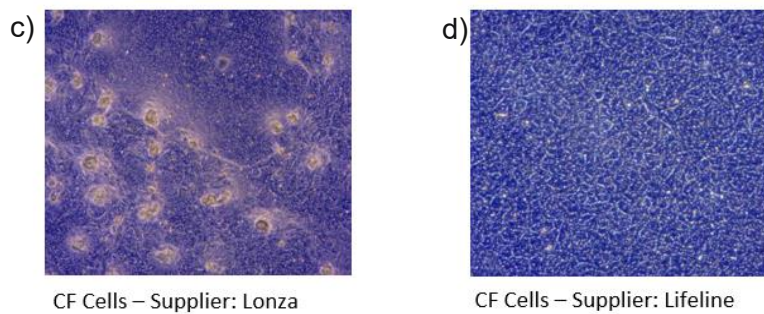


Figure 20 Differences in cell supply – ~90% Confluency was achieved in almost all tested cell vials after b) 5 days, a) but cells provided by BioIVT needed an extended expansion period of 12 days. c),d) Different cell sources were more or less likely to attach to the membrane and remain attached.

When donor 450918 was grown in ALI medium, the cell layer was very stretched and stressed. Many dead cells were present on top of the cell monolayer and the culture appeared "cloudy". Cells of this donor grown in Leiden medium showed cobblestone cell morphology but were completely overgrown. Despite all that, sparse ciliation and mucus production were present in both conditions (fig 19,20).

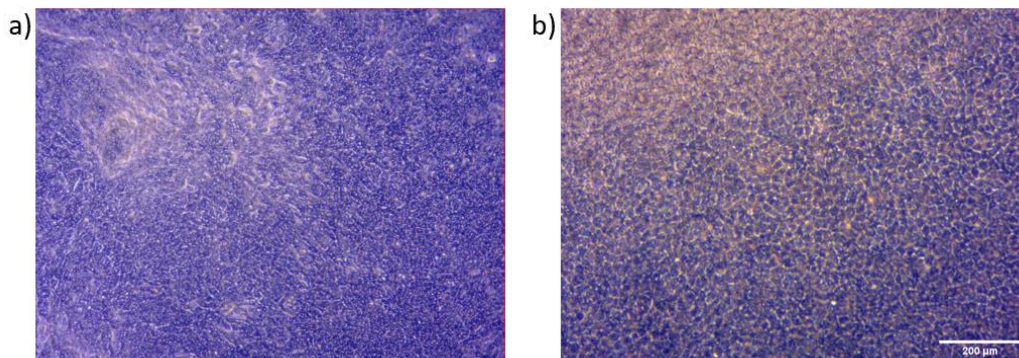


Figure 21 phase contrast image of donor 450918 a) in ALI medium, revealing "cloudy spots" and stretched cells b) in Leiden medium, showing overgrowth but beautiful cobblestone morphology

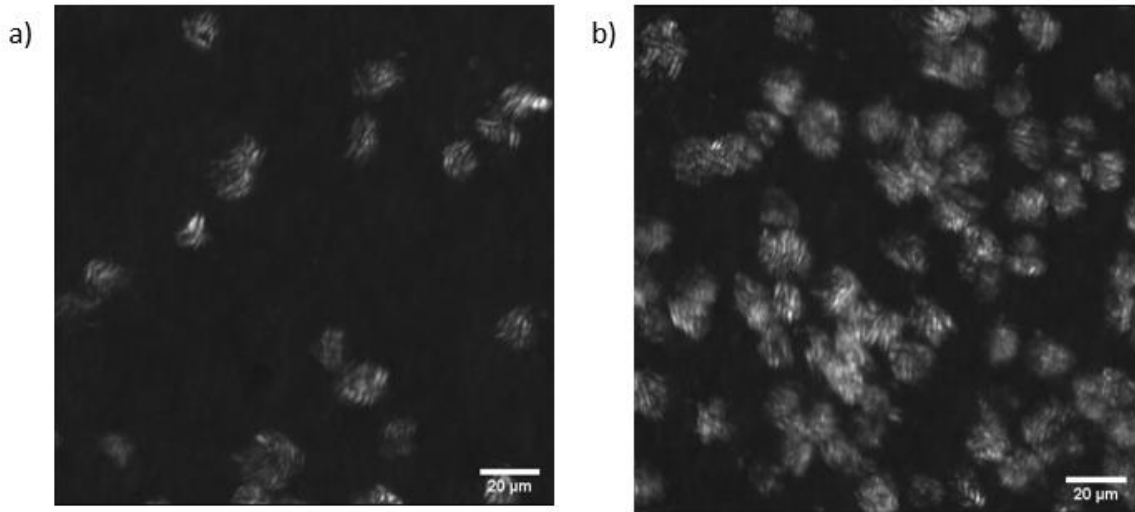


Figure 22 motion detection images of cilia a) at 15 days of ALI in ALI medium b) at 15 days on ALI in Leiden medium
Primary cells of donor 450918 were then seeded on collagen IV coated organ chips with PET membrane and 3 µm pore PDMS membrane in both medium conditions. The cells growing on PDMS retracted immediately after the introduction of ALI, whereas CF cells growing on PET could be maintained on the chip for up to 15 days (fig 21,22).

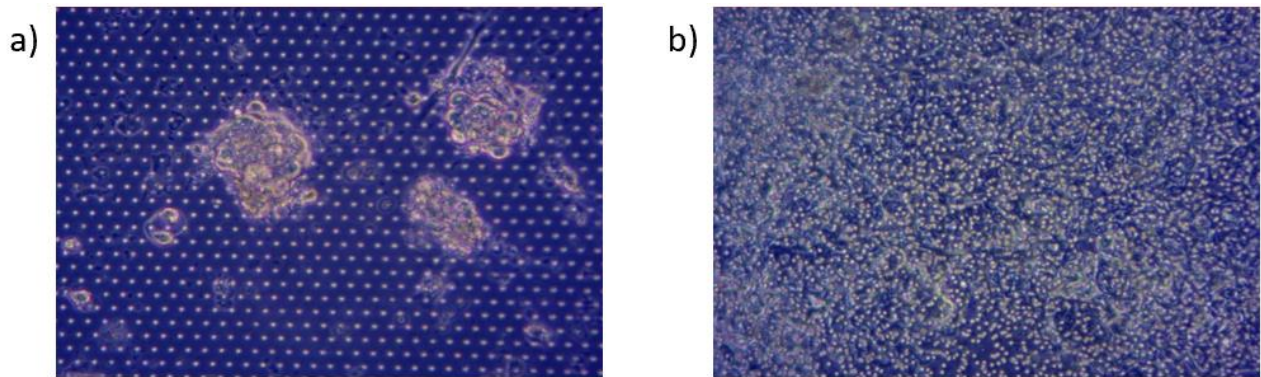


Figure 23 a) cells retracting from PDMS membrane b) cells attached to PET membrane, but a few clusters of dead cells are present

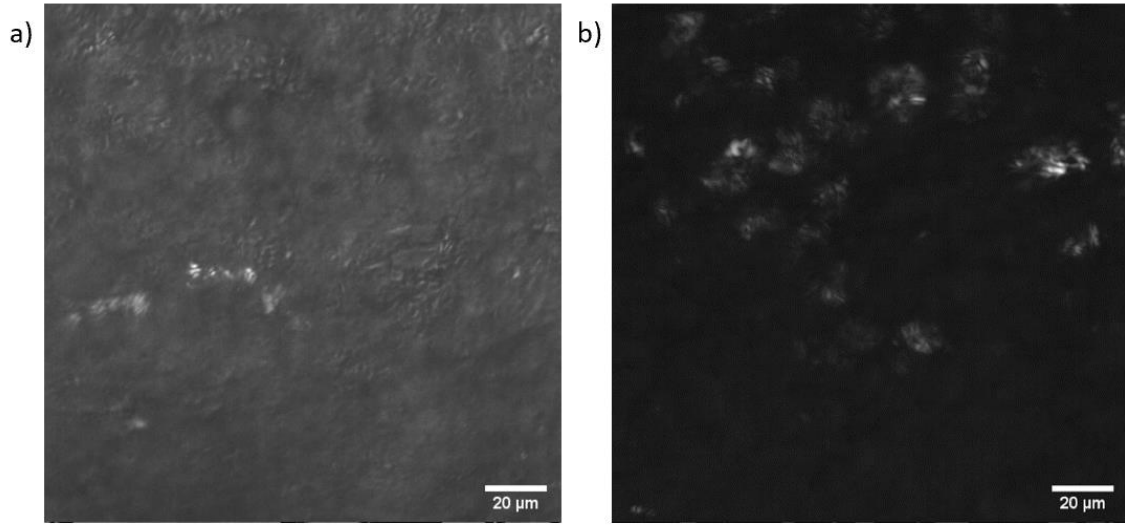


Figure 24 motion detection images reveal ciliation on day 15 of ALI on PET Chip a) Leiden medium b) ALI medium

Due to a shortage in cell supply, the screening process was reinitiated, and culturing of donor FC-0103 underwent optimization. Hence FC-0103 cells were seeded on collagen IV coated transwells, and different media conditions were tested. Leiden medium and ALI medium served as control, and Leiden medium with only 20% of supplement hEGF was tested to tackle overgrowth. In addition, two other media conditions were designed to find the golden mean between Leiden medium that shows cobblestone cell morphology, but heavy overgrowth and ALI medium that lead to stretched, flat, and squamous cells but higher cilia density. Therefore, hEGF was left out and replaced with 2% KnockOut serum in one condition and 4% Serum (2% KnockOut Serum replacement and 2% HyClone fetal bovine serum) in the other. There were no major differences observed between all adjusted conditions (fig 23 a). Low ciliation, cell death, patches of cobblestone cell morphology but also flat, squamous, and stretched cells, reduction of overgrowth were found in all of these conditions. Cell death also appeared in healthy controls in these media.

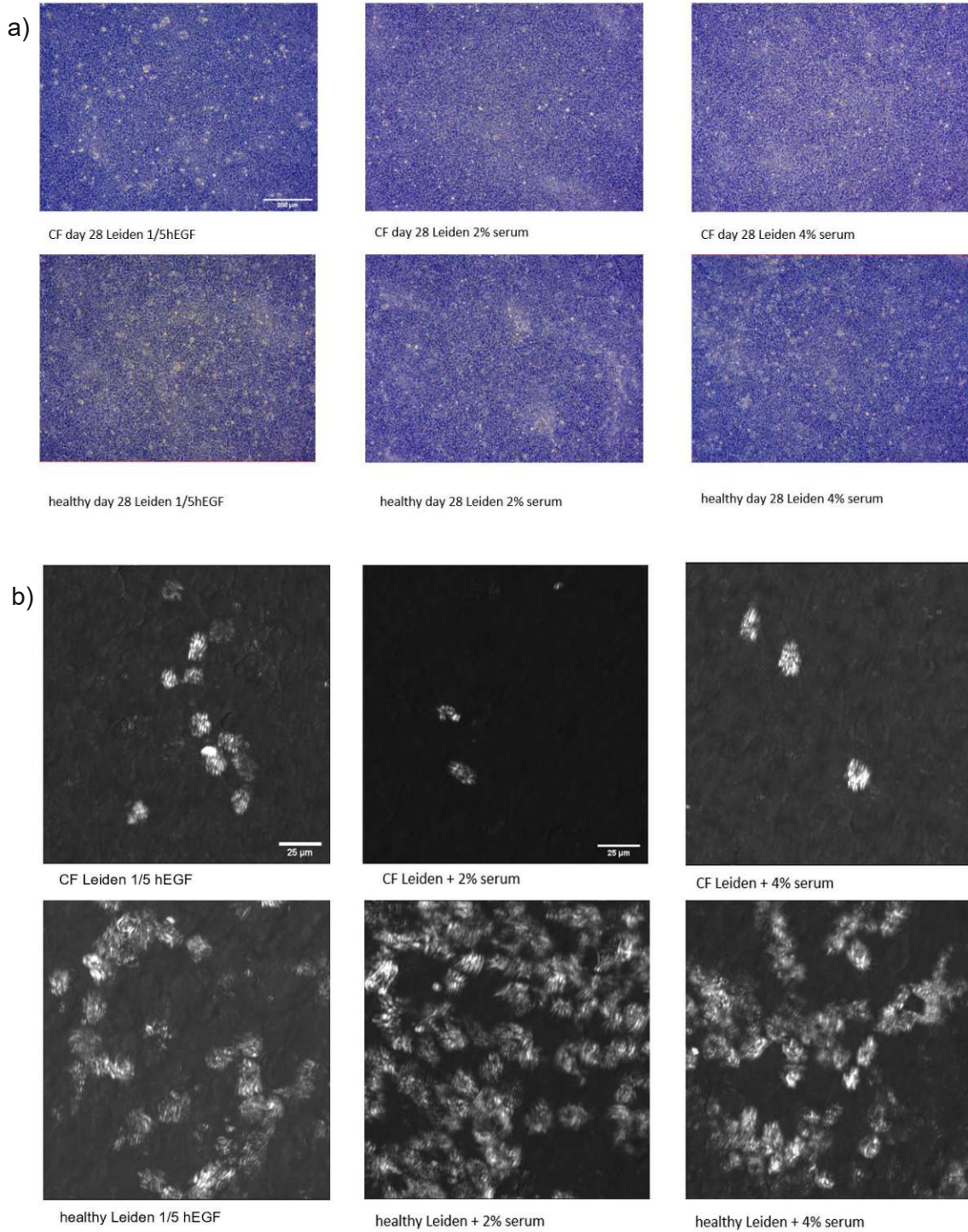


Figure 25 a) phase-contrast images of transwell cultures in different media conditions reveal no major difference in influence on cell morphology; b) Motion detection images reveal differences in cilia density. All CF cultures in the 3 different media conditions show very low differentiation at 25 days on ALI compared to the control conditions that show high cilia coverage.

To further improve cell culture conditions, the use of collagen I gel coated with collagen IV instead of collagen IV coating alone was assessed for its ability to influence cell differentiation and viability positively. Therefore, 8 mg/mL collagen gels were prepared for transwells, tested for their pH, and stamped down to a height of 200 μm . All previously tested media conditions were investigated on these gels. In all these conditions, but Leiden 1/5 hEGF, cilia already appeared after 5 days of air liquid interface. The cultures were as densely ciliated as the healthy control by day 25 of ALI. Cells in Leiden 1/5 medium died after the introduction of ALI. Although ciliation improved drastically in all other conditions, patches of stretched cells remained, and holes formed within the cell monolayer. Therefore, collagen I gel concentration was decreased to test whether a decrease in gel stiffness would influence the formation of holes and the morphology of cells. The concentrations of 8 mg/mL, 5 mg/mL, and 3 mg/mL were tested in ALI medium and PneumaCult medium (during this experiment, parallel experiments in the optimization study for the healthy airway model yielded good results for the use of PneumaCult – see above). Almost no holes were visible at a collagen I concentration of 3 mg/mL, and cilia density was similar to 8 mg/mL collagen I gel (fig 24). These two gels were subsequently tested in the Open Top Chip, as the open chamber allows for easy gel introduction onto the culture membrane as compared to the closed off S-1 chip. At a higher concentration of collagen, the gel remained attached to the chamber of the Open Top, but holes were formed in the cell monolayer (fig 25). The reverse is true for low collagen I concentrations. No cultures could be kept alive for more than 7 days in the Open Top Chip.

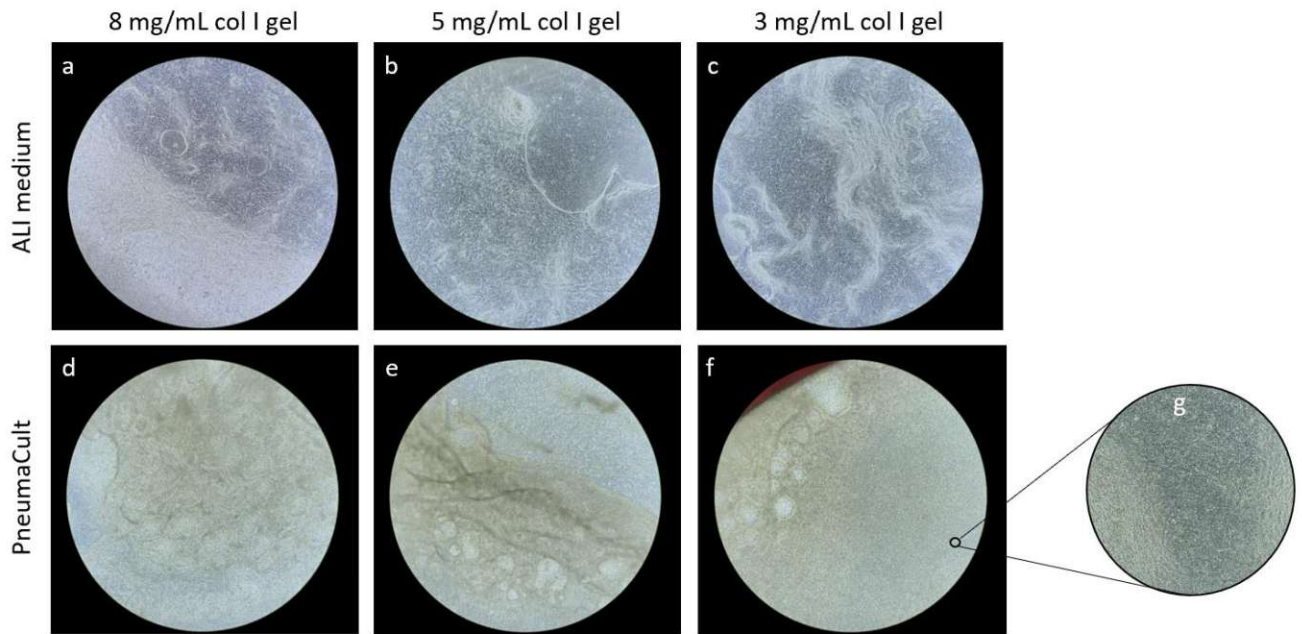


Figure 26 . a), d) Big holes in the cell layer appear right after the introduction of ALI and do not close in 8 mg/mL collagen I gels in CF transwell cultures at 25 days of air liquid interface. Cells retract from the membrane in collagen I gels with b), e) 5 mg/mL and c), f) 3 mg/mL. g) Best morphology was observed in undetached 3 mg/mL collagen I gel in PneumaCult medium.

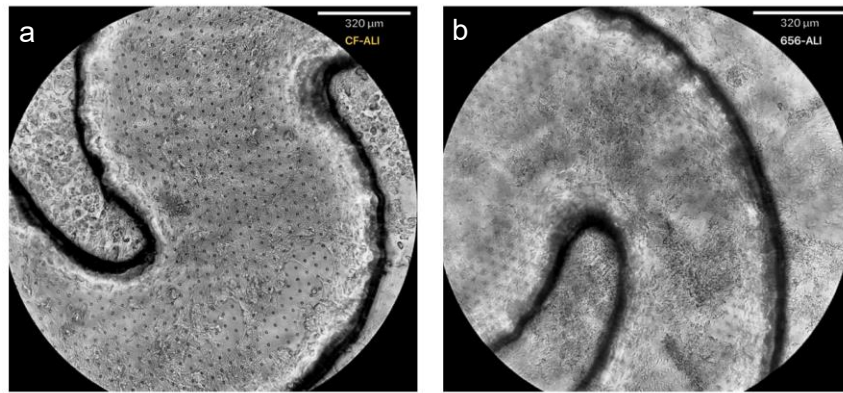


Figure 27 Open Top cell cultures grown on 8 mg/mL collagen I gel in ALI medium. Both a) CF and b) healthy control show holes and patches of squamous and dead cells.

After successfully introducing gel into the standard S1-Chip with 7µm pore PDMS membrane and differentiation of healthy cells to a mucociliary endothelium, it was assessed whether the platform switch from Open Top to S1-Chip for Cystic Fibrosis would benefit the Cystic Fibrosis culture. Although the chips with PET membranes yielded better results, the favored chip is the S-1 chip as it is commercially available and hence widely accessible. The gel forms a barrier between the membrane and the cells, direct contact is therefore minimized and substrate stiffness is tunable.

Based on previous findings described in the healthy lung chip, collagen I/IV gels were introduced into the S1-Chip, and CF cells were seeded either in PneumaCult or ALI medium on top of the gel. Whereas cells growing in PneumaCult medium formed a monolayer, cells grown in ALI medium detached from the membrane and finally underwent cell death (fig 26).

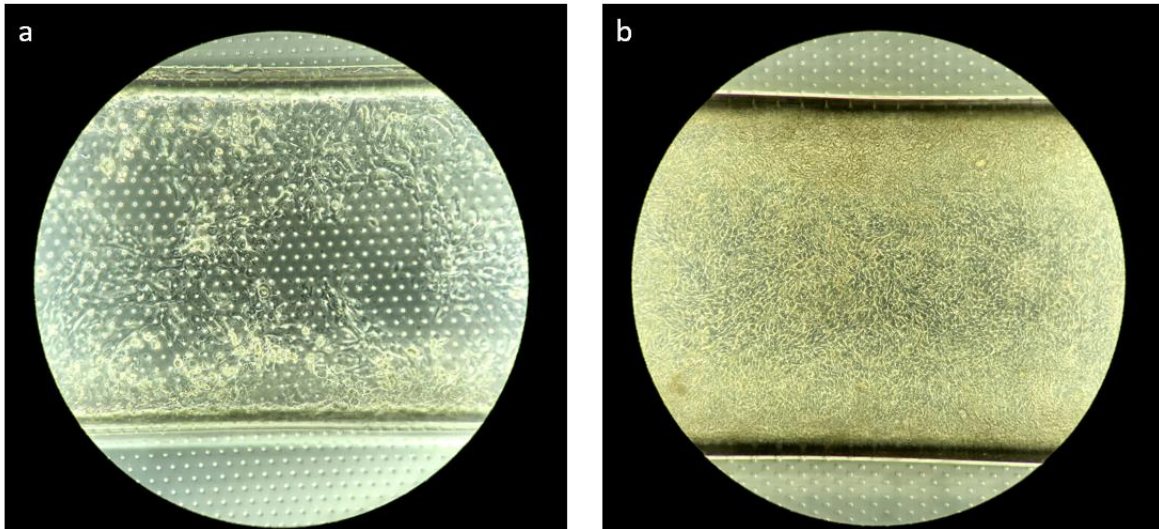


Figure 28 S1-Chip CF culture at 7 days post-ALI on collagen I/IV gels a) cultured in ALI medium b) cultured in PneumaCult medium

The cell cultures in PneumaCult medium differentiated, showing ciliation and mucus secretion as well as all major cell types such as goblet cells, ciliated cells, and basal cells of the airway epithelium already at 14 days of ALI (fig 27). Nevertheless, it should be mentioned that the gel retracted from the membrane at both the inlet and outlet side, but the center remained attached to the walls. At 21 days, post-ALI bead assays were performed and confirmed the functioning of the mucociliary escalator as well as a high cilia density comparable to the healthy control (fig 28).

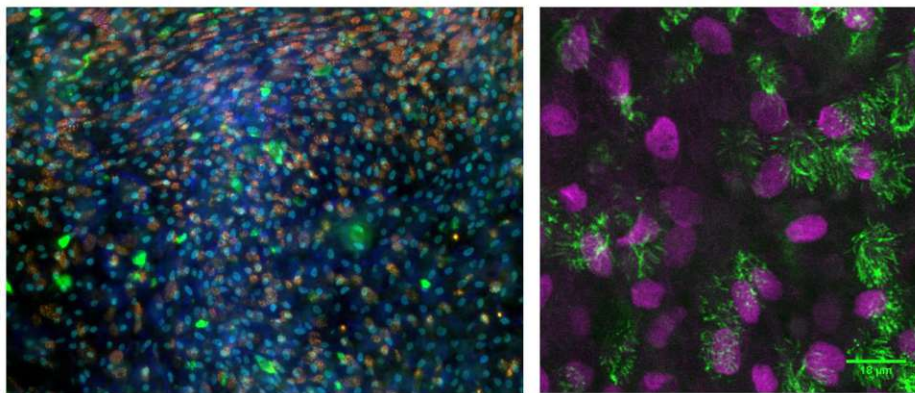


Figure 29 Validation of epithelial differentiation at 14 days post-ALI; a) goblet cells in green, ciliated cells in orange, basal cells in light blue and actin in dark blue; b) basal cells in magenta and ciliated cells in green

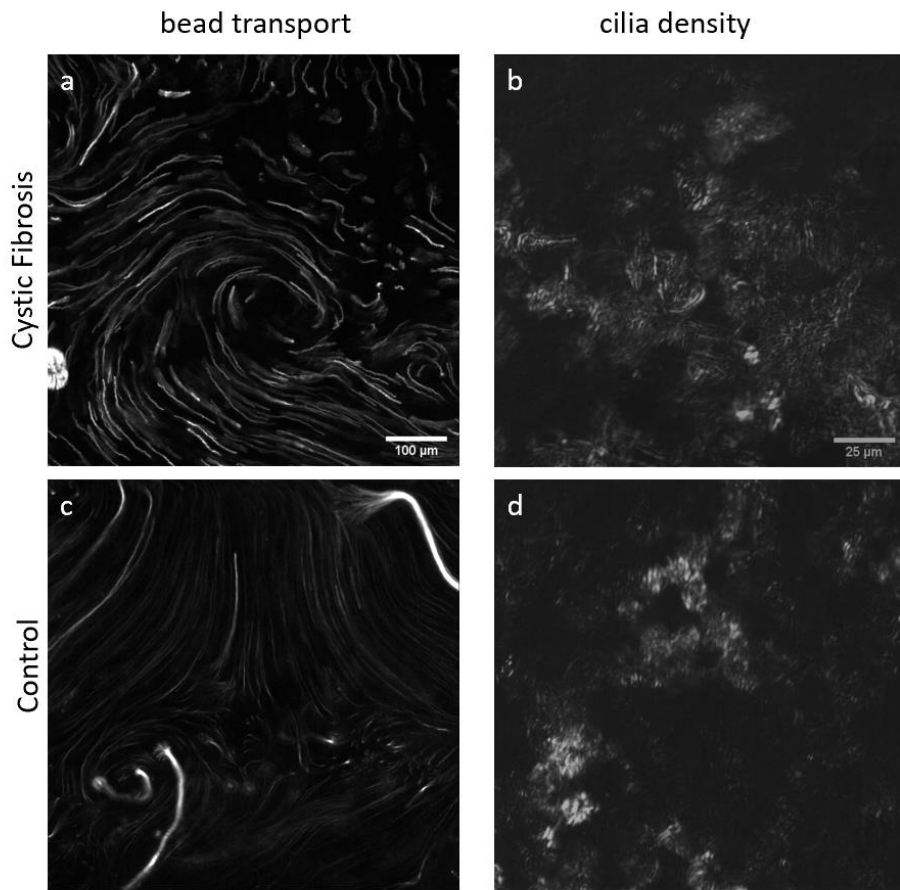


Figure 30 Visualization of the mucociliary escalator and cilia density at 21 days on ALI. a) The bead flow in the CF culture show vortex and short trajectories. c) The trajectories in the control chips follow long streamlines. b) cilia coverage in CF cells is comparable to control d).

4 Discussion

Organs-on-a-chip are complex human cell-culture platforms that aim to mimic human biology more closely than conventional cell culture models and thus add to the toolbox of translational research. A precisely defined and tunable microenvironment is crucial in model development to ensure reproducibility and relevance. This microenvironment includes the cell types involved, their hierarchy, the tissue architecture, mechanical forces, and fluid flow experienced *in vivo*. Therefore, forces experienced within an automated cell culture system containing the organ chips, as used in this work, and the forces experienced in the native tissue milieu must be determined and balanced. This is critical for lung tissue at air liquid interface, where the lumen experiences

airflow and stretch and the endothelium experiences blood flow. Here, the top channel containing the epithelium was kept static in air, and the medium was perfused through the bottom channel. The buildup of the effluent medium in the outlet reservoir is pushing with increasing force against the membrane that does not experience hydrostatic pressure from the top channel. These forces have to be balanced to prevent an environment that can lead to inflammation, fibroblast proliferation, remodeling, and ultimately the disruption of the epithelium. However, these manifestations of epithelia on organ chips can also appear due to improper cell isolation, ECM conditions and medium formulations. Thus, it is not straightforward to discriminate between parameters and find the root source causing these observations. Hence, two or more parameters were tested in different combinations, and controls for each parameter were designed based on provided protocols. Once a parameter could be narrowed down to benefit cell viability, cell morphology, differentiation and adhesion, the controls for subsequent experiments were refined. The composition and stiffness of the extracellular matrix are crucial for the success of cell cultures. Drastic differences in cell morphology and attachment were observed.

Interestingly, bovine serum albumin yielded the best results in ECM coating experiments prior to using gels. This might be attributed to its hydrophilic properties and hydrophobic pockets[75] but would require further study. Notwithstanding cell attachment to BSA coated chips, invasion occurs and patches of cell movement appear next to areas of cobblestone morphology. The introduction of gel to stop cells from invading the bottom channel by blocking the pores of the PDMS membrane has proven to be highly successful. Both gels containing collagen and gels containing Matrigel plus collagen successfully stopped epithelial cells from migrating into the vascular channel. Nonetheless, collagen gels are preferred over gels containing Matrigel because of its ill-defined composition. Continued optimization of the gels is desirable to assess which gel composition, concentration, and resulting stiffnesses favor primary epithelial cell cultures both for healthy cells as well as cells derived from Cystic Fibrosis patients. The analysis and adaptation of the mesh sizes of the different gel networks could allow neutrophil transmigration from the vascular channel through the gel to the epithelium. Moreover, the presence of gel enables mimicry of connective tissue by embedding fibroblasts. To establish the base model, including epithelium and endothelium, the next step would consist of optimizing ECM coating for endothelial cells in the bottom channel, optimal shear rates for endothelial differentiation, and the optimization of co-culture medium. The medium found to sustain both healthy and Cystic Fibrosis cells has to be adopted to maintain endothelial cells. A starting point would be the use of PneumaCult medium,

proven to support epithelium culture on the chips, and the supplementation of endothelial growth factors, first and foremost vascular endothelial growth factor (VEGF).

The optimized protocol for the healthy airway chip and the newly established epithelial model for Cystic Fibrosis on the S1-Chip will require further characterization to apply it as a research model. Baselines for biomarker expression, such as proinflammatory cytokines TNF-alpha, IL- β , IL-8 and IL-6, must be identified and confirmed to be situated within or near the ranges found *in vivo* using qPCR and ELISA. Several donors should be tested to prove the robustness of the optimized protocol and exclude sensitivity based on donor-to-donor variability. Regarding the Cystic Fibrosis disease model, it would be commendable to include donors with different genetic backgrounds and treatment histories.

The introduction of microelectrodes to the chip or the integration of passive methods to assess CFTR function would extend the possibilities of readouts on the CF chip. Electrophysiological measurements (Ussing chamber experiments) are used to test CFTR potentiator and corrector drugs that aim to enhance or restore CFTR function. In addition, the establishment of the quantification of mucociliary clearance as a general readout, can be an important measure to understand the cystic fibrosis lung and could be used to assess the efficacy of drugs that reduce mucus viscosity, such as Dornase alpha. Pattern recognition applied on the acquired high speed videos and algorithms leading to automated quantification of cilia density, ciliary beat, cilia alignment, bead transport, flow directionality would enable the detailed characterization of the mucociliary escalator. Finally, as newer findings [62] suggest that cyclic strain and airflow lead to an altered inflammatory marker expression and cell type composition, those mechanical cues should be assessed for their potential of fine-tuning CF phenotypes on chips.

This research was conducted in 2019, and since then, several lung-on-a-chip models were developed hosting healthy lung epithelium from different regions of the lung, nevertheless models hosting Cystic Fibrosis patient-derived cells are missing[56]. This reflects the necessity and underlines the novelty of a Cystic Fibrosis lung-on-a-chip.

5 Conclusion

Organs-on-a-chip platforms open exciting new windows for foundational and translational medicine, by combining cutting-edge cell culture methods with microfluidics, thereby allowing the precise manipulation of the mechanochemical environment of the native human tissue. As human diseases can only be studied *in vivo* in model animals that don't recapitulate human physiology,

this technology will enable an unprecedented insight into human disease mechanisms at the tissue level and set a milestone in animal welfare in research. Cystic Fibrosis is a deadly disease with very limited treatment options and understanding pathogenesis and disease mechanisms is desperately needed. The possibility to decompose the complex interplay of the involved tissue, the immune response and pathogen interaction through a top-down process enables subsequent selection of specific factors and the integration of those into a bottom-up model to increase complexity to a level where research questions focusing on particular and systemic interactions can be addressed. This will lead to a more wholesome understanding and knowledge of the disease. The human lung is a dynamic environment and mechanical forces are shaping the tissue function. The impeded mucociliary clearance, limited airflow and altered stretching behavior of the lung are hallmarks in Cystic Fibrosis. Using the new possibilities that come with microfluidic cell culture, such as stretch of the cell layers as well as air and fluid flow will help us understand the role of the altered mechanical forces acting in disease progression and, which is currently only possible to a certain degree. Hence, human Cystic Fibrosis Organs-on-a-chip will shape the future in foundational research and treatment as well as take a pivotal role in the pharmaceutical industry.

6 References

- [1] F. Ratjen, S. C. Bell, S. M. Rowe, C. H. Goss, A. L. Quittner, and A. Bush, "Cystic fibrosis," *Nature Reviews Disease Primers*, vol. 1, p. 15010 EP-, 2015, doi: 10.1038/nrdp.2015.10.
- [2] C. R. Esther *et al.*, "Mucus accumulation in the lungs precedes structural changes and infection in children with cystic fibrosis," *Science translational medicine*, vol. 11, no. 486, 2019, doi: 10.1126/scitranslmed.aav3488.
- [3] S. E. Birket *et al.*, "A functional anatomic defect of the cystic fibrosis airway," *American journal of respiratory and critical care medicine*, vol. 190, no. 4, pp. 421–432, 2014, doi: 10.1164/rccm.201404-0670OC.
- [4] J. K. Gustafsson *et al.*, "Bicarbonate and functional CFTR channel are required for proper mucin secretion and link cystic fibrosis with its mucus phenotype," *J Exp Med*, vol. 209, no. 7, pp. 1263–1272, 2012, doi: 10.1084/jem.20120562.
- [5] J. V. Fahy and B. F. Dickey, "Airway mucus function and dysfunction," *The New England journal of medicine*, vol. 363, no. 23, pp. 2233–2247, 2010, doi: 10.1056/NEJMra0910061.
- [6] E. Puchelle, O. Bajolet, and M. Abély, "Airway mucus in cystic fibrosis," *Paediatric respiratory reviews*, vol. 3, no. 2, pp. 115–119, 2002, doi: 10.1016/S1526-0550(02)00005-7.
- [7] A. Oliver, R. Cantón, P. Campo, F. Baquero, and J. Blázquez, "High Frequency of Hypermutable *Pseudomonas aeruginosa* in Cystic Fibrosis Lung Infection," *Science (New York, N.Y.)*, vol. 288, no. 5469, pp. 1251–1253, 2000, doi: 10.1126/science.288.5469.1251.
- [8] R.-J. Shei, J. E. Peabody, N. Kaza, and S. M. Rowe, "The epithelial sodium channel (ENaC) as a therapeutic target for cystic fibrosis," *Current opinion in pharmacology*, vol. 43, pp. 152–165, 2018, doi: 10.1016/j.coph.2018.09.007.
- [9] B. Button *et al.*, "A periciliary brush promotes the lung health by separating the mucus layer from airway epithelia," *Science (New York, N.Y.)*, vol. 337, no. 6097, pp. 937–941, 2012, doi: 10.1126/science.1223012.
- [10] D. J. Hassett *et al.*, "*Pseudomonas aeruginosa* biofilm infections in cystic fibrosis: insights into pathogenic processes and treatment strategies," *Expert opinion on therapeutic targets*, vol. 14, no. 2, pp. 117–130, 2010, doi: 10.1517/14728220903454988.
- [11] X. X. Tang *et al.*, "Acidic pH increases airway surface liquid viscosity in cystic fibrosis," *Journal of Clinical Investigation*, vol. 126, 2016, doi: 10.1172/JCI83922.
- [12] A. R. Berkebile and P. B. McCray, "Effects of airway surface liquid pH on host defense in cystic fibrosis," *The international journal of biochemistry & cell biology*, vol. 52, pp. 124–129, 2014, doi: 10.1016/j.biocel.2014.02.009.
- [13] A. A. Pezzulo *et al.*, "Reduced airway surface pH impairs bacterial killing in the porcine cystic fibrosis lung," *Nature*, vol. 487, no. 7405, pp. 109–113, 2012, doi: 10.1038/nature11130.
- [14] S. Rao and J. Grigg, "New insights into pulmonary inflammation in cystic fibrosis," *Archives of disease in childhood*, vol. 91, no. 9, pp. 786–788, 2006, doi: 10.1136/adc.2004.069419.
- [15] L. S. Mott *et al.*, "Progression of early structural lung disease in young children with cystic fibrosis assessed using CT," *Thorax*, vol. 67, no. 6, pp. 509–516, 2012, doi: 10.1136/thoraxjnl-2011-200912.

- [16] H. Heijerman, "Infection and inflammation in cystic fibrosis: a short review," *Journal of cystic fibrosis : official journal of the European Cystic Fibrosis Society*, vol. 4 Suppl 2, pp. 3–5, 2005, doi: 10.1016/j.jcf.2005.05.005.
- [17] B. Kerem *et al.*, "Identification of the cystic fibrosis gene: genetic analysis," *Science (New York, N.Y.)*, vol. 245, no. 4922, pp. 1073–1080, 1989.
- [18] J. R. Riordan *et al.*, "Identification of the cystic fibrosis gene: cloning and characterization of complementary DNA," *Science (New York, N.Y.)*, vol. 245, no. 4922, pp. 1066–1073, 1989.
- [19] J. M. Rommens *et al.*, "Identification of the cystic fibrosis gene: chromosome walking and jumping," *Science (New York, N.Y.)*, vol. 245, no. 4922, pp. 1059–1065, 1989.
- [20] "ACOG Committee Opinion No. 486: Update on carrier screening for cystic fibrosis," *Obstetrics and gynecology*, vol. 117, no. 4, pp. 1028–1031, 2011, doi: 10.1097/AOG.0b013e31821922c2.
- [21] J. E. Mickle and G. R. Cutting, "GENOTYPE-PHENOTYPE RELATIONSHIPS IN CYSTIC FIBROSIS," *Medical Clinics of North America*, vol. 84, no. 3, pp. 597–607, 2000, doi: 10.1016/S0025-7125(05)70243-1.
- [22] A. Iwasaki, E. F. Foxman, and R. D. Molony, "Early local immune defences in the respiratory tract," *Nat Rev Immunol*, vol. 17, no. 1, pp. 7–20, Jan. 2017, doi: 10.1038/nri.2016.117.
- [23] P. D. Sly *et al.*, "Risk Factors for Bronchiectasis in Children with Cystic Fibrosis," *N Engl J Med*, vol. 368, no. 21, pp. 1963–1970, May 2013, doi: 10.1056/NEJMoa1301725.
- [24] M. A. Khan, Z. S. Ali, N. Sweezey, H. Grasemann, and N. Palaniyar, "Progression of Cystic Fibrosis Lung Disease from Childhood to Adulthood: Neutrophils, Neutrophil Extracellular Trap (NET) Formation, and NET Degradation," *Genes (Basel)*, vol. 10, no. 3, p. 183, Feb. 2019, doi: 10.3390/genes10030183.
- [25] R. W. Vandivier *et al.*, "Elastase-mediated phosphatidylserine receptor cleavage impairs apoptotic cell clearance in cystic fibrosis and bronchiectasis," *J Clin Invest*, vol. 109, no. 5, pp. 661–670, Mar. 2002, doi: 10.1172/JCI113572.
- [26] C. M. de Bont, W. J. H. Koopman, W. C. Boelens, and G. J. M. Pruijn, "Stimulus-dependent chromatin dynamics, citrullination, calcium signalling and ROS production during NET formation," *Biochimica et Biophysica Acta (BBA) - Molecular Cell Research*, vol. 1865, no. 11, Part A, pp. 1621–1629, Nov. 2018, doi: 10.1016/j.bbamcr.2018.08.014.
- [27] I. Bianconi *et al.*, "Persistence and Microevolution of *Pseudomonas aeruginosa* in the Cystic Fibrosis Lung: A Single-Patient Longitudinal Genomic Study," *Frontiers in Microbiology*, vol. 9, p. 3242, 2019, doi: 10.3389/fmicb.2018.03242.
- [28] C. Alvarez-Ortega and C. S. Harwood, "Responses of *Pseudomonas aeruginosa* to low oxygen indicate that growth in the cystic fibrosis lung is by aerobic respiration," *Mol Microbiol*, vol. 65, no. 1, pp. 153–165, Jul. 2007, doi: 10.1111/j.1365-2958.2007.05772.x.
- [29] O. Ciofu and T. Tolker-Nielsen, "Tolerance and Resistance of *Pseudomonas aeruginosa* Biofilms to Antimicrobial Agents-How *P. aeruginosa* Can Escape Antibiotics," *Front Microbiol*, vol. 10, pp. 913–913, May 2019, doi: 10.3389/fmicb.2019.00913.
- [30] J. M. PILEWSKI and R. A. FRIZZELL, "Role of CFTR in Airway Disease," *Physiological Reviews*, vol. 79, no. 1, pp. S215–S255, Jan. 1999, doi: 10.1152/physrev.1999.79.1.S215.

- [31] A. McCarron, M. Donnelley, and D. Parsons, "Airway disease phenotypes in animal models of cystic fibrosis," *Respir Res*, vol. 19, no. 1, pp. 54–54, Apr. 2018, doi: 10.1186/s12931-018-0750-y.
- [32] B. H. Rosen *et al.*, "Infection Is Not Required for Mucoinflammatory Lung Disease in CFTR-Knockout Ferrets," *Am J Respir Crit Care Med*, vol. 197, no. 10, pp. 1308–1318, May 2018, doi: 10.1164/rccm.201708-1616OC.
- [33] M. Brodlie *et al.*, "Primary bronchial epithelial cell culture from explanted cystic fibrosis lungs," *Experimental Lung Research*, vol. 36, no. 2, pp. 101–110, Mar. 2010, doi: 10.3109/01902140903165265.
- [34] H.-W. Snoeck, "Modeling human lung development and disease using pluripotent stem cells," *Development*, vol. 142, no. 1, pp. 13–16, Jan. 2015, doi: 10.1242/dev.115469.
- [35] M. A. Lancaster and J. A. Knoblich, "Organogenesis in a dish: Modeling development and disease using organoid technologies," *Science*, vol. 345, no. 6194, p. 1247125, Jul. 2014, doi: 10.1126/science.1247125.
- [36] J. F. Dekkers *et al.*, "A functional CFTR assay using primary cystic fibrosis intestinal organoids," *Nature medicine*, vol. 19, no. 7, pp. 939–945, 2013, doi: 10.1038/nm.3201.
- [37] N. Sachs *et al.*, "Long-term expanding human airway organoids for disease modeling," *EMBO J.*, vol. 38, no. 4, Feb. 2019, doi: 10.15252/embj.2018100300.
- [38] K. H. Benam, M. Mazur, Y. Choe, T. C. Ferrante, R. Novak, and D. E. Ingber, "Human Lung Small Airway-on-a-Chip Protocol," *Methods in molecular biology (Clifton, N.J.)*, vol. 1612, pp. 345–365, 2017, doi: 10.1007/978-1-4939-7021-6_25.
- [39] D. Huh, Y. Torisawa, G. A. Hamilton, H. J. Kim, and D. E. Ingber, "Microengineered physiological biomimicry: organs-on-chips," *Lab Chip*, vol. 12, no. 12, pp. 2156–2164, Jun. 2012, doi: 10.1039/c2lc40089h.
- [40] J. C. Nawroth, R. Barrile, D. Conegliano, S. van Riet, P. S. Hiemstra, and R. Villenave, "Stem cell-based Lung-on-Chips: The best of both worlds?," *Advanced drug delivery reviews*, 2018, doi: 10.1016/j.addr.2018.07.005.
- [41] K. Ronaldson-Bouchard and G. Vunjak-Novakovic, "Organs-on-a-Chip: A Fast Track for Engineered Human Tissues in Drug Development," *Cell stem cell*, vol. 22, no. 3, pp. 310–324, 2018, doi: 10.1016/j.stem.2018.02.011.
- [42] D. Huh, B. D. Matthews, A. Mammoto, M. Montoya-Zavala, H. Y. Hsin, and D. E. Ingber, "Reconstituting organ-level lung functions on a chip," *Science*, vol. 328, no. 5986, pp. 1662–1668, Jun. 2010, doi: 10.1126/science.1188302.
- [43] L. G. Griffith and M. A. Swartz, "Capturing complex 3D tissue physiology in vitro," *Nat. Rev. Mol. Cell Biol.*, vol. 7, no. 3, pp. 211–224, Mar. 2006, doi: 10.1038/nrm1858.
- [44] D. Lu and G. S. Kassab, "Role of shear stress and stretch in vascular mechanobiology," *J R Soc Interface*, vol. 8, no. 63, pp. 1379–1385, Oct. 2011, doi: 10.1098/rsif.2011.0177.
- [45] P. F. Davies, "Flow-mediated endothelial mechanotransduction," *Physiol. Rev.*, vol. 75, no. 3, pp. 519–560, Jul. 1995, doi: 10.1152/physrev.1995.75.3.519.
- [46] P. F. Davies, C. F. Dewey, S. R. Bussolari, E. J. Gordon, and M. A. Gimbrone, "Influence of hemodynamic forces on vascular endothelial function. In vitro studies of shear stress and pinocytosis in bovine aortic cells," *J. Clin. Invest.*, vol. 73, no. 4, pp. 1121–1129, Apr. 1984, doi: 10.1172/JCI111298.

- [47] M. Levesque, "Vascular endothelial cell proliferation in culture and the influence of flow," *Biomaterials*, vol. 11, no. 9, pp. 702–707, Nov. 1990, doi: 10.1016/0142-9612(90)90031-K.
- [48] V. K. Sidhaye, K. S. Schweitzer, M. J. Caterina, L. Shimoda, and L. S. King, "Shear stress regulates aquaporin-5 and airway epithelial barrier function," *Proc Natl Acad Sci U S A*, vol. 105, no. 9, pp. 3345–3350, Mar. 2008, doi: 10.1073/pnas.0712287105.
- [49] V. D. Varner, J. P. Gleghorn, E. Miller, D. C. Radisky, and C. M. Nelson, "Mechanically patterning the embryonic airway epithelium," *Proc Natl Acad Sci USA*, vol. 112, no. 30, p. 9230, Jul. 2015, doi: 10.1073/pnas.1504102112.
- [50] J. Li, Z. Wang, Q. Chu, K. Jiang, J. Li, and N. Tang, "The Strength of Mechanical Forces Determines the Differentiation of Alveolar Epithelial Cells," *Dev. Cell*, vol. 44, no. 3, pp. 297–312.e5, 05 2018, doi: 10.1016/j.devcel.2018.01.008.
- [51] Z. Tang *et al.*, "Mechanical Forces Program the Orientation of Cell Division during Airway Tube Morphogenesis," *Dev. Cell*, vol. 44, no. 3, pp. 313–325.e5, 05 2018, doi: 10.1016/j.devcel.2017.12.013.
- [52] K. H. Benam *et al.*, "Small airway-on-a-chip enables analysis of human lung inflammation and drug responses in vitro," *Nat. Methods*, vol. 13, no. 2, pp. 151–157, Feb. 2016, doi: 10.1038/nmeth.3697.
- [53] L. M. Ince, M. Pariollaud, and J. E. Gibbs, "Lung physiology and defense," *Current Opinion in Physiology*, vol. 5, pp. 9–15, Oct. 2018, doi: 10.1016/j.cophys.2018.04.005.
- [54] R. J. Mason, "Thoughts on the alveolar phase of COVID-19," *American Journal of Physiology-Lung Cellular and Molecular Physiology*, vol. 319, no. 1, pp. L115–L120, Jul. 2020, doi: 10.1152/ajplung.00126.2020.
- [55] L. Si *et al.*, "A human-airway-on-a-chip for the rapid identification of candidate antiviral therapeutics and prophylactics," *Nat Biomed Eng*, May 2021, doi: 10.1038/s41551-021-00718-9.
- [56] H. L. Ogden, H. Kim, K. A. Wikenheiser-Brokamp, A. P. Naren, and K. S. Mun, "Cystic Fibrosis Human Organs-on-a-Chip," *Micromachines*, vol. 12, no. 7, p. 747, Jun. 2021, doi: 10.3390/mi12070747.
- [57] A. P. Nesmith, A. Agarwal, M. L. McCain, and K. K. Parker, "Human airway musculature on a chip: an in vitro model of allergic asthmatic bronchoconstriction and bronchodilation," *Lab Chip*, vol. 14, no. 20, pp. 3925–3936, Aug. 2014, doi: 10.1039/C4LC00688G.
- [58] B. A. Hassell *et al.*, "Human Organ Chip Models Recapitulate Orthotopic Lung Cancer Growth, Therapeutic Responses, and Tumor Dormancy In Vitro," *Cell Reports*, vol. 21, no. 2, pp. 508–516, Oct. 2017, doi: 10.1016/j.celrep.2017.09.043.
- [59] L. Nardo, G. Maritz, R. Harding, and S. B. Hooper, "Changes in lung structure and cellular division induced by tracheal obstruction in fetal sheep," *Exp Lung Res*, vol. 26, no. 2, pp. 105–119, Mar. 2000, doi: 10.1080/019021400269907.
- [60] Z. Liu *et al.*, "MAPK-Mediated YAP Activation Controls Mechanical-Tension-Induced Pulmonary Alveolar Regeneration," *Cell Reports*, vol. 16, no. 7, pp. 1810–1819, Aug. 2016, doi: 10.1016/j.celrep.2016.07.020.
- [61] J. R. Beitler, A. Malhotra, and B. T. Thompson, "Ventilator-Induced Lung Injury," *Clin Chest Med*, vol. 37, no. 4, pp. 633–646, Dec. 2016, doi: 10.1016/j.ccm.2016.07.004.

- [62] J. C. Nawroth *et al.*, “Breathing on Chip: studying the effect of biomechanical forces on airway epithelial cell biology using a modular Airway Lung-Chip,” presented at the European Organ-on-a-Chip Society Conference 2021, online, Jul. 2021.
- [63] K. H. Benam, M. Königshoff, and O. Eickelberg, “Breaking the *In Vitro* Barrier in Respiratory Medicine. Engineered Microphysiological Systems for Chronic Obstructive Pulmonary Disease and Beyond,” *Am J Respir Crit Care Med*, vol. 197, no. 7, pp. 869–875, Apr. 2018, doi: 10.1164/rccm.201709-1795PP.
- [64] J. Shrestha *et al.*, “Lung-on-a-chip: the future of respiratory disease models and pharmacological studies,” *Critical Reviews in Biotechnology*, vol. 40, no. 2, pp. 213–230, Feb. 2020, doi: 10.1080/07388551.2019.1710458.
- [65] A. Jain *et al.*, “Primary Human Lung Alveolus-on-a-chip Model of Intravascular Thrombosis for Assessment of Therapeutics,” *Clin. Pharmacol. Ther.*, vol. 103, no. 2, pp. 332–340, Feb. 2018, doi: 10.1002/cpt.742.
- [66] D. Huh *et al.*, “A Human Disease Model of Drug Toxicity–Induced Pulmonary Edema in a Lung-on-a-Chip Microdevice,” *Sci. Transl. Med.*, vol. 4, no. 159, pp. 159ra147–159ra147, Nov. 2012, doi: 10.1126/scitranslmed.3004249.
- [67] A. Varone *et al.*, “A novel organ-chip system emulates three-dimensional architecture of the human epithelia and the mechanical forces acting on it,” *Biomaterials*, vol. 275, p. 120957, Aug. 2021, doi: 10.1016/j.biomaterials.2021.120957.
- [68] D. Huh *et al.*, “Microfabrication of human organs-on-chips,” *Nat Protoc*, vol. 8, no. 11, pp. 2135–2157, Nov. 2013, doi: 10.1038/nprot.2013.137.
- [69] Christopher G. Sip and A. Folch, “Stable chemical bonding of porous membranes and poly(dimethylsiloxane) devices for long-term cell culture”.
- [70] S. H. Randell, M. L. Fulcher, W. O’Neal, and J. C. Olsen, “Primary epithelial cell models for cystic fibrosis research,” *Methods in molecular biology (Clifton, N.J.)*, vol. 742, pp. 285–310, 2011, doi: 10.1007/978-1-61779-120-8_18.
- [71] J. Schindelin *et al.*, “Fiji: an open-source platform for biological-image analysis,” *Nat. Methods*, vol. 9, no. 7, pp. 676–682, Jun. 2012, doi: 10.1038/nmeth.2019.
- [72] K. Jaqaman *et al.*, “Robust single-particle tracking in live-cell time-lapse sequences,” *Nat. Methods*, vol. 5, no. 8, pp. 695–702, Aug. 2008, doi: 10.1038/nmeth.1237.
- [73] A. Mata, A. J. Fleischman, and S. Roy, “Characterization of polydimethylsiloxane (PDMS) properties for biomedical micro/nanosystems,” *Biomed Microdevices*, vol. 7, no. 4, pp. 281–293, Dec. 2005, doi: 10.1007/s10544-005-6070-2.
- [74] R. Kalluri and R. A. Weinberg, “The basics of epithelial-mesenchymal transition,” *J Clin Invest*, vol. 119, no. 6, pp. 1420–1428, Jun. 2009, doi: 10.1172/JCI39104.
- [75] B. X. Huang, H.-Y. Kim, and C. Dass, “Probing three-dimensional structure of bovine serum albumin by chemical cross-linking and mass spectrometry,” *Journal of the American Society for Mass Spectrometry*, vol. 15, no. 8, pp. 1237–1247, Aug. 2004, doi: 10.1016/j.jasms.2004.05.004.

7 Table of figures

Figure 1: Comparison of experimental strategies for lung modeling taken from Nawroth et al. 2018 [40]. Whereas animal models enable in vivo studies, they do not resemble human physiology and, in particular, diseased phenotypes. High maintenance efforts and the ethical need to minimize the use of animals lower the throughput of studies. The Lung-on-Chip uses human cells that can be patient-specific and incorporates differentiated epithelium and endothelium as well as circulating immune cells. The microfluidic channels in the chip create tissue-tissue interfaces and mimic the in vivo hemodynamic environment. The complexity and novelty of the chip reduce the throughput and familiarity. Organoid cultures self-assemble and allow the study of patient-derived airway epithelium. The spheroid shape with an internal lumen excludes infection modeling and the study of mucociliary clearance. Air exposed primary cells in transwell cultures have standardized culture protocols and are easy to use. Transwell cultures are highly characterized and allow the use of patient-specific cells. The static culture model does not mimic the mechanical microenvironment crucial for complete differentiation, especially for endothelial cells. 2D submerged cell lines are of great use for CFTR-related research but highly limited for translational research..... 15

Figure 2 Branching and epithelial composition of the human lung [53] 17

Figure 3 a); b) barrier chip by Benam et al. [63] c) thin film airway musculature by Nesmith et al.[57] 19

Figure 4: Steps in model development 20

Figure 5: Cell Culture Platforms a) S1-Chip Design with PET or PDMS membrane b) Open Top Chip Design with PDMS membrane c) transwell with PET membrane d) S1-Chip in chip carrier..... 21

Figure 6: Emulate S1-Chip with Airway Culture: The top channel and bottom channel are separated by a 7 µm pore PDMS membrane. The top channel houses the mucociliary airway epithelium and microvascular endothelium is seeded to the bottom channel. Both channels can be perfused with different fluids/air and at different flowrates..... 22

Figure 7 The Human Emulation System Components Pod, Zoë and Orb 23

Figure 8 Schematic flow circuit for one channel 24

Figure 9 Basic Primary Airway Epithelial Culture. Primary cells are expanded in T75 flasks and harvested after 5 days. The cells are seeded onto the culture platforms and kept submerged for 3 days. Afterward, an air liquid interface is introduced to start the differentiation process that lasts for 21 days.....25

Figure 10 Timeline of Airway Chip culture. Before seeding cells onto the chip, the chip is activated by rendering membrane hydrophilic during the last day of expansion and coated with ECM. Cells are seeded onto the chip and the chips are connected to Zoë. After 3 days of medium perfusion in both channels, air liquid interface is established by introducing air to the top channel.....25

Figure 11 ECM conditions. The primary airway epithelial cells reacted drastically differently to each ECM condition. Best results were observed with BSA coating, and worst results were obtained using collagen I and collagen IV, as seen in the representative phase-contrast images. Where BSA shows cobblestone morphology and collagen I/IV either detaches or shows EMT.....39

Figure 12 A 100-fold higher retinoic acid concentration than in regular transwell cultures improves cell viability and differentiation. Both at a) 7 days and b) 14 days on ALI the 100-fold higher concentration shows the best quality control ranking.c) This is also confirmed by LDH photometry on day 14.40

Figure 13 Scores 7 days after Introduction of ALI for several medium conditions tested in one experiment with 4 chips per condition. Conditions – red: ALI medium; blue: DMEM/HEPES + Leiden supplements; yellow: D-valine DMEM/F12/BEBM (1:1) + Leiden supplements; purple: D-valine DMEM/F12 + ALI supplements; white: PneumaCult ALI; green: Leiden 1/5 hEGF + Y-compound41

Figure 14 phase-contrast images of cells grown in a) D-valine Leiden b) PneumaCult c) ALI medium41

Figure 15 Staining of healthy culture growing on collagen I/IV gel in the S1-Chip; a) cell nuclei in blue (DAPI), goblet cells in green (Muc5AC), ciliated cells in magenta (alpha-tubulin); b) cell nuclei in blue (DAPI), goblet cells in green (Muc5AC), ciliated cells in orange (alpha-tubulin); club cells in red (CC16)42

Figure 16 Motion detection revealed a) a functioning mucociliary escalator and b) cilia beating and heigh cilia coverage.....43

Figure 17 LDH levels of effluent - PRE = flow onset 2 hours after seeding; Post = flow onset 6 hours after seeding and refreshment of medium after 4 hours.....43

Figure 18 Comparison of pressures in top and bottom channel. A 1 mL medium plug in the top channel reservoirs balances the pressure due to the waste building up in the reservoirs for up to 32h. Empirically, up to 72h of continuous perfusion (and waste buildup) was supported with this protocol, likely because the cellular barrier function adds sufficient resistance to withstand the pressure differential up to this point.44

Figure 19 Average score for each pressure condition on 14 days of ALI (N=4 chips). Pressure experiments were performed in Leiden 1/5 hEGF. Conditions, A: 1.88 mL (inlet plug) and 1.91 mL (outlet reservoir) plug; B: 1 mL plug and daily waste removal; C: 1 mL plug; D: 200 μ L plug; E: 1 mL plug in 1:1 Leiden 1/5 hEGF medium and Leiden 1/5 hEGF conditioned in transwell culture of same the same donor. See attachment 5.....45

Figure 20 Differences in cell supply – ~90% Confluency was achieved in almost all tested cell vials after b) 5 days, a) but cells provided by BioIVT needed an extended expansion period of 12 days. c),d) Different cell sources were more or less likely to attach to the membrane and remain attached.....46

Figure 21 phase contrast image of donor 450918 a) in ALI medium, revealing "cloudy spots" and stretched cells b) in Leiden medium, showing overgrowth but beautiful cobblestone morphology46

Figure 22 motion detection images of cilia a) at 15 days of ALI in ALI medium b) at 15 days on ALI in Leiden medium47

Figure 23 a) cells retracting from PDMS membrane b) cells attached to PET membrane, but a few clusters of dead cells are present47

Figure 24 motion detection images reveal ciliation on day 15 of ALI on PET Chip a) Leiden medium b) ALI medium48

Figure 25 a) phase-contrast images of transwell cultures in different media conditions reveal no major difference in influence on cell morphology; b) Motion detection images reveal differences in cilia density. All CF cultures in the 3 different media conditions show very low differentiation at 25 days on ALI compared to the control conditions that show high cilia coverage.....49

Figure 26 . a), d) Big holes in the cell layer appear right after the introduction of ALI and do not close in 8 mg/mL collagen I gels in CF transwell cultures at 25 days of air liquid interface. Cells retract from the membrane in collagen I gels with b), e) 5 mg/mL and c), f) 3 mg/mL. g) Best morphology was observed in undetached 3 mg/mL collagen I gel in PneumaCult medium.51

Figure 27 Open Top cell cultures grown on 8 mg/mL collagen I gel in ALI medium. Both a) CF and b) healthy control show holes and patches of squamous and dead cells.51

Figure 28 S1-Chip CF culture at 7 days post-ALI on collagen I/IV gels a) cultured in ALI medium b) cultured in PneumaCult medium52

Figure 29 Validation of epithelial differentiation at 14 days post-ALI; a) goblet cells in green, ciliated cells in orange, basal cells in light blue and actin in dark blue; b) basal cells in magenta and ciliated cells in green52

Figure 30 Visualization of the mucociliary escalator and cilia density at 21 days on ALI. a) The bead flow in the CF culture show vortex and short trajectories. c) The trajectories in the control chips follow long streamlines. b) cilia coverage in CF cells is comparable to control d).53

8 Attachments

ATTACHMENT 1

Scoring Chart

Attachment/Feature	Image 1	Image 2	Image 3	Image 4	Description	Score
Attachment/Peeling					The epithelium forms a monolayer throughout the chip	3
					The epithelium looks rather ok and forms a monolayer almost completely throughout the chip, some gaps, visible or slight spots of voids are filled with cells.	3
Movement					The epithelium forms a monolayer completely throughout the chip although cells are struggling with attachment and may look strange because of this.	4
					Some parts (ca. 20%) of the epithelium show signs of movement: stretched cells that align to each other	5
Overgrowth					Cells have a stable size morphology, monolayer looks regular	5
					Approx. 50% of the epithelium has stretched and/or aligned cells.	5
Invasion					Cells form a monolayer that is well visible	6
					Invasion: Presence of cells on top of epi-layer	6

- 1 Cell Death
- 2 Ciliation
- 3 Attachment
- 4 Movement/Shape
- 5 Overgrowth
- 6 Invasion

Feature	Image 1	Image 2	Image 3	Image 4	Description	Score
Cell death					No death cells are visible on top of the cell layer	6
					Cell death is only visible on the side channels that are not on ALL	3
Ciliation					Cilia are present throughout the epithelial layer but low amount	6
					Cell death is visible as part of the epi-layer (resulting in gaps etc.)	3

ATTACHMENT 2

Scoring heat map - 5 days on ALI (Donor 656) - ECM coating

Read-out date: 2018-11-09



Left tray

Ciliation	Attachm	Move-	Over-	Invasion	Cell
peeling	ment	ment	growth		death
3	0	1	1	1	0
3	2	1	1	1	3
3	0	1	1	1	0
3	0	1	1	1	0
3	0	1	1	1	0
3	0	1	1	1	0

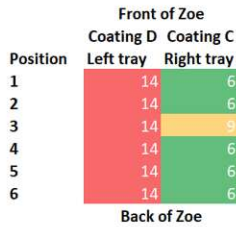
Right tray

Ciliation	Attachm	Move-	Over-	Invasion	Cell
peeling	ment	ment	growth		death
3	0	1	1	1	2
3	0	1	1	1	2
3	0	1	1	1	2
3	0	1	1	1	2
3	0	1	1	1	2
3	0	1	1	1	2

Zoe: 128

Incubator: 1

Read-out date: 2018-11-09



Left tray

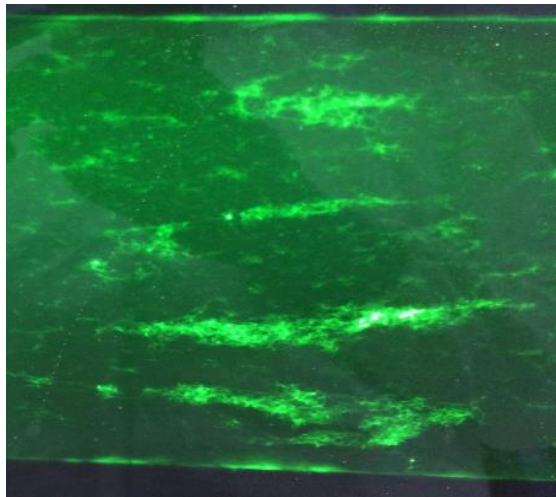
Ciliation	Attachm	Move-	Over-	Invasion	Cell
peeling	ment	ment	growth		death
3	3	3	1	1	3
3	3	3	1	1	3
3	3	3	1	1	3
3	3	3	1	1	3
3	3	3	1	1	3
3	3	3	1	1	3

Right tray

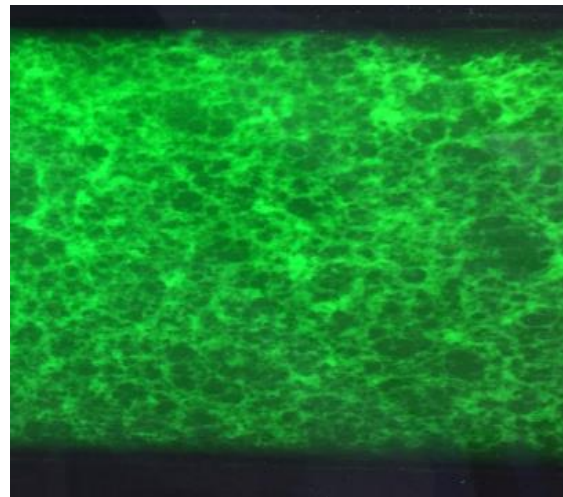
Ciliation	Attachm	Move-	Over-	Invasion	Cell
peeling	ment	ment	growth		death
3	0	0	1	0	2
3	0	0	1	0	2
3	2	0	1	0	3
3	0	0	1	0	2
3	0	0	1	0	2
3	0	0	1	0	2

ATTACHMENT 3

Gel attachment to PDMS membrane (stained and imaged by Colleague Ibra Moulana)



Collagen IV gel (1 mg/mL)



Collagen IV (400 µg/mL) + Matrigel (200 µg/mL)

ATTACHMENT 4

Scoring heat map of healthy S1 gel conditions

Condition	Chip ID	Days Post-ALI	Peeling	Cell death	Overgrowth	Movement	Ciliation	Invasion	Score
Matrigel + Collagen IV	1.1	14	0	1	1	2.5	0	1	5.5
Matrigel + Collagen IV	1.2	14	1	1	1	2	0	0.5	5.5
Matrigel + Collagen IV	1.3	14	0	0	2	3	0	0	5
Matrigel + Collagen IV	1.4	14	2	0	2	3	0	1	8
Matrigel + Collagen IV	1.6	14	0	1	2	2.5	0	3	8.5
Matrigel + Collagen IV	1.1	14	0.5	0	1	2	0	0	3.5
Matrigel + Collagen IV	1.4	14	0	1	2	0.5	0	0	3.5
Matrigel + Collagen IV	1.6	14	2	0	0	2	0	0	4
Matrigel + Collagen IV	1.7	14	0	2	1	2	0	0	5
Matrigel + Collagen IV	1.8	14	1.5	1	1	2	1	2	8.5
Matrigel + Collagen IV	1.9	14	1	1	0	3	0	3	8
Collagen IV	2.3	14	0	1	1	2	0	1	5
Collagen IV	2.4	14	1	0	0	3	2	0	6
Collagen IV	2.5	14	0.5	0	1	1	0	0	2.5
Collagen IV	2.6	14	0	0	1	1	0	1	3
Collagen IV	2.9	14	1	0	2	2	0	0	5
Collagen I + IV	2.1	14	0	1.5	2	1	0	0.5	5
Collagen I + IV	2.4	14	0	1.5	2	2.5	0	1.5	7.5
Collagen I + IV	2.5	14	2	1	2	2.5	0	0	7.5
Collagen I + IV	2.6	14	1	1.5	1	2.5	0	1	7
Control	3.1	14	2	1	2	1	0	3	9
Control	3.2	14	0	0	3	1	0	1	5
Control	3.3	14	2	0	2	3	0	1.5	8.5
Control	3.8	14	2	0	3	2	0	3	10
Control	3.1	14	0.5	0	0.5	1	0	0	2
Control	3.2	14	0	2	1	2	0	2	7
Control	3.3	14	0	2	0	2	0	2	6
Control	3.5	14	0	0.5	0	2	0	2	4.5

ATTACHMENT 5

Scoring heat map of pressure experiments at 14 days of ALI

